Electronic supplementary information

Stereochemistry of Coordination Polyhedra *vs.* Single Ion Magnetism in Penta- and Hexacoordinated Co(II) Complexes with Tridentate Rigid Ligand

Barbora Brachňaková[a], Simona Matejová,[a] Ján Moncol,[a] Radovan Herchel,[b] Ján Pavlik,[a] Eufemio Moreno-Pineda,[c] Mario Ruben,[c,d] Ivan Šalitroš[a,b,e]*

a) Department of Inorganic Chemistry. Faculty of Chemical and Food Technology. Slovak University of Technology in Bratislava. Bratislava SK-81237, Slovakia. *e-mail: ivan.salitros@stuba.sk
b) Department of Inorganic Chemistry. Faculty of Science, Palacký University, 17. listopadu 12, 771 46 Olomouc, Czech Republic
c) Institut für Nanotechnologie, Karlsruher Institut für Technologie, Postfach 3640, Karlsruhe 76021. Germany;
d) Institute de Physique et Chimie de Matériaux de Strasbourg (IPCMS), CNRS-Université de Strasbourg, 23, rue du Loess, BP 43 67034 Strasbourg cedex 2, France
e) Central European Institute of Technology, Brno University of Technology, Purkyňova 123, 61200 Brno Czech Republic

Contents

S1 Synthesis and Spectral Characterization of Reported Compounds

Experimental section

Materials and methods

3,5-di-*tert*-butylbenzyl bromide, $CoCl_2.6H_2O$, $CoBr_2.6H_2O$, KNCS, ethanol, acetonitrile and diethyl ether were used as received without any further purification. Dimethylsulfoxide (DMSO) solvent has been dried over CaH_2 a distilled prior to use. The starting material 2,6-bis(1*H*-benzimidazol-2-yl)pyridine was prepared by published methods.[18] IR spectra were measured by the ATR technique or in KBr pellets in 4000 – 400 cm^{-1} region (Magna FTIR 750. Nicolet). Electronic spectra were recorded in the acetonitrile solutions at the concentration $\approx 10^{-4}$ mol dm^{-3} on Specord 250 plus Analytical Jena in the range of 800 – 200 nm. Elemental analysis of carbon, hydrogen and nitrogen was carried out by an automated analyser (Vario Micro Cube). The microcrystalline solid of complexes **1**-**4** were measured by Philips PW 1730/1050 (Bragg – Brentano geometry, Co-Kα radiation, 40kV/35mA, range of 2Θ 3-52°, step 0.02°) diffractometer .

Synthesis of 2,6-Bis(1-(3,5-di-tert-butylbenzyl)-1H-benzimidazol-2-yl)pyridine (L)

The preparation of ligand is visualised on Scheme 1. 50 mL two-necked round-bottom flask was charged with 2,6-bis(benzimidazol-2-yl)pyridine (1.0 g, 3.21 mmol, 1eq) and dissolved in 10 mL DMSO. The crushed KOH (1.08 g, 19.2 mmol, 6eq) was added into the solution and suspension was stirred for 1 hour at room temperature under nitrogen atmosphere. 3,5-di-*tert*-butyl-benzyl bromide (1.84g, 6.4 mmol, 2eq) was dissolved in 2 mL anhydrous DMSO and added over the stirring of suspension. The reaction mixture was stirred at 60°C for 20 hours and cooled down to room temperature, DMSO solvent was removed by vacuum distillation, the residue was treated with distilled water (50 mL) and extracted with $CHCl_3$ (3 x 200 mL). The chloroform was removed using a rotary evaporator and the oily residue was column chromatographed on silica gel with $CHCl_3$/ethyl acetate (4:1) as an eluent. The main product L was isolated as first fraction (R_f = 0.31) in 61% yield (1.40 g, 1.96 mmol) as white powder. The side-product of this reaction, 2-(6-(1*H*-benzimidazol-2-yl)pyridin-2-yl)-1-(3,5-di-*tert*-butylbenzyl)-1*H*-benzimidazole, was collected as the second and more polar fraction (R_f = 0.12) in 15% yield (0.25 g, 0.49 mmol) as white powder.
Disubstituted product L: **^{1}H NMR** (400 MHz, d^6-DMSO, 25 °C, δ/ppm): 8.37 (d, *J* = 7.64 Hz, 2H), 8.25 (dd, *J* = 8.49, 7.26 Hz, 1H), 7.78 (dd, *J* = 9.29, 4.84 Hz, 4H), 7.67 (dd, *J* = 7.13 Hz, 1.23 Hz, 4H), 7.32 (pd, *J*=7.20, 1.27 , 4H), 7.14 (t, *J*=1.60 Hz, 2H), 6.74 (d, *J*= 1.64, 4H), 5.75 (s, 4H), 0.99 (s, 36H). ^{13}C NMR (125 MHz, d6-DMSO, 25 °C, δ/ppm): 150.4 (C14), 149.6 (C3), 149.3 (C4), 142.3 (C5), 138.8 (C1), 136.5 (C10), 136.4 (C12), 125.3 (C2), 123.4 (C8), 122.6 (C7), 120.8 (C15), 120.3 (C13), 119.6 (C6), 111.3 (C9), 47.5 (C11), 34.2 (C16), 30.9 (C17). **Elemental analysis** for $C_{49}H_{57}N_5$ (M_w = 716.01 g mol^{-1}) found % (expected %): C 81.56 (82.19); N 8.86 (9.78); H 7.6 (8.02).**FT−IR** (ATR, $\tilde{\nu}_{max}/cm^{-1}$): 3055 (w, C-$H_{ar}$); 2954, 2904, 2865 (w, C-H_{alif}); 1597, 1572 (m, C-C_{ar} a C_{ar}-N); **UV - VIS** (acetonitrile, λ/nm, 2.10^{-5} mol.L^{-1}): 218 (π → π*), 327 (n → π*).
Monosubstituted side-product L1: **^{1}H NMR** (300 MHz, d^6-DMSO, 25 °C, δ/ppm): 12.88 (s, 1H), 8.45 (dd, *J* = 7.7, 0.8 Hz, 1H), 8.37 – 8.11 (m, 2H), 8.05 (d, *J* = 8.1 Hz, 1H), 7.81 (dd, *J* = 12.2, 7.7 Hz, 2H), 7.66 (d, *J* = 7.4 Hz, 1H), 7.44 (t, *J* = 7.2 Hz, 1H), 7.39-7.26 (m, 3H), 7.11 (s, 1H), 6.88 (d, *J* = 1.6 Hz, 2H), 6.35 (s, 2H), 0.98 (s, 18H). **^{13}C NMR** (75 MHz, d^6-DMSO, 25 °C, δ/ppm): 150.30(C_q), 150.16(C_q), 150.02(C_q), 149.25(C_q), 148.03(C_q), 143.86(C_q), 142.17(C_q), 138.73(CH), 136.95(C_q), 136.75(C_q), 134.99(C_q), 125.20(CH), 123.59(CH), 123.50(CH), 122.66(CH), 122.19(CH), 121.97(CH), 121.25(CH), 120.70(CH), 119.76(CH), 119.49(CH), 112.20(CH), 111.33(CH), 48.24(CH_2), 34.14(C_q), 30.85(CH_3). **Elemental analysis** for $C_{34}H_{35}N_5$ (M_w = 513.68 g mol^{-1}) found % (expected %): C 77.35 (79.50); N 13.63 (17.53); H 3.99 (6.87).**FT−IR** (ATR, $\tilde{\nu}_{max}/cm^{-1}$): 3370 (w, N-

H); 3054 (w, C-H_{ar});2953, 2904, 2864 (w, C-H_{alif}); 1596, 1572 (m, C-C_{ar} a C_{ar}-N). **UV - VIS** (acetonitrile, λ/nm, 2.10^{-5} mol·L^{-1}): 222 (π → π*), 327 (n → π*).

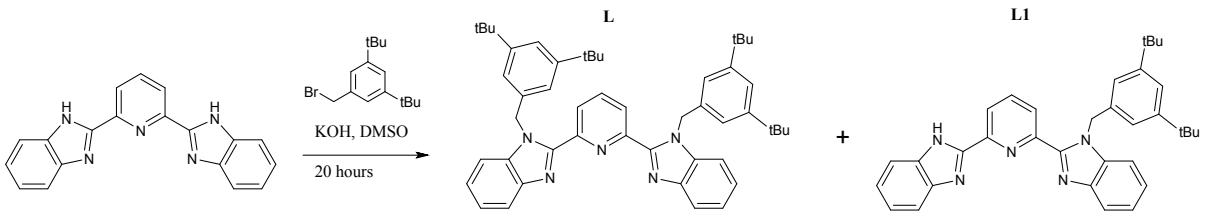

Scheme 1 Preparation of ligands L and L1

Preparation of Co(II) complexes

Complex **1** $[Co(L)(NCS)_2]$

Ligand L (50 mg, 0.069 mmol, 1.0 eq) was dissolved in 20 mL acetonitrile and heated at 82°C for 30 minutes. Solution of cobalt(II) isothiocyanate was prepared *in situ* by mixing of cobalt(II) chloride hexahydrate (18.3 mg, 0.077 mmol, 1.1 eq) and potassium thiocyanate (0.015mg, 0.154 mmol, 2.2 eq) in 4 mL ethanol. Suspension was filtered in order to remove the potassium chloride and mother liquor was added to the ligand solution and refluxed 48 hours. Green precipitation of **1** in the microcrystalline form was filtered off and mother liquor was submitted for the slow evaporation at RT which allowed to obtain the single-crystals within few days. **Elemental analysis** for $C_{51}H_{57}CoN_7S_2$ (M_w = 891.10 g mol^{-1}) found % (expected %): C 68.01 (68.74); N 10.09 (11.00); H 5.95 (6.45) S 6.99 (7.20). **FT−IR** (ATR, $\tilde{\nu}_{max}/cm^{-1}$): 3060 (w, C-$H_{ar}$), 2962 (w, C-$H_{alif}$), 2864 (w, C-$H_{alif}$), 2070, 2052 (s, N=C=S), 1600,1504 (m, C-C_{ar} a C_{ar}-N). **UV - VIS** (acetonitrile, λ/nm, 2.10^{-5} mol·L^{-1}): 317 (π → π*), 345 (n → π*).

Complexes **2** $[Co(L)Cl_2]$ and **3** $[Co(L)Br_2]$

Cobalt(II) chloride hexahydrate (33.2 mg, 0.154 mmol, 1.1 eq) or cobalt(II) bromide hexahydrate (49.6 mg, 0.152 mmol, 1.1 eq) was added into the acetonitrile solution (30 mL) of ligand L (100 mg, 0.138 mmol, 1eq). Reaction mixture was refluxed for 48 hours, the green precipitation of microcrystalline form of **2** or **3** was filtered of and mother liquor was submitted for the slow crystallization at RT which allowed to obtain the single-crystals within few days. Complexes **2**: **Elemental analysis** for $C_{49}H_{57}Cl_2CoN_5$ (M_w = 845.85 g mol^{-1}) found % (expected %): C 68.07 (69.79); N 8.07 (8.28); H 6.92 (6.79). **FT−IR** (ATR, $\tilde{\nu}_{max}/cm^{-1}$): 3062 (w, C-$H_{ar}$), 2955, 2904, 2866 (w, C-H_{alif}), 1599, 1568, 1514 (m, C-C_{ar} a C_{ar}-N). **UV – VIS** (acetonitrile, λ/nm, 1.10^{-5} mol·L^{-1}): 313 (π → π*), 338 (n → π*). Complexes **3**: **Elemental analysis** for $C_{49}H_{57}Br_2CoN_5$ (M_w = 934.75 g mol^{-1}) found % (expected %): C 62.17 (62.96); N 7.49 (7.46); H 6.40 (6.15). **FT−IR** (ATR, $\tilde{\nu}_{max}/cm^{-1}$): 3048 (w, C-$H_{ar}$), 2958, 2900, 2866 (w, C-H_{alif}), 1599,1566, 1514 (m, C-C_{ar} a C_{ar}-N). **UV – VIS** (acetonitrile, λ/nm, 1.10^{-5} mol·L^{-1}): 313 (π → π*), 348 (n → π*).

Complex **4** $[Co(L)_2]Br_2.2CH_3OH.H_2O$

Cobalt(II) bromide hexahydrate (15.5 mg, 0.065 mmol, 1 eq) was added into the methanol solution (30 mL) of ligand L (100 mg, 0.138 mmol, 2.12 eq). Reaction mixture was refluxed for 48 hours, the yellow solution was filtered and retained for the slow crystallization at room temperature. The yellowish single-crystals suitable for the X-ray diffraction analysis were collected after several days. **Elemental analysis** for $C_{100}H_{124}Br_2CoN_{10}O_3$ (M_w = 1732.83 g mol^{-1}) found % (expected %): C 69.02 (69.31); N 7.96 (8.08); H 7.11 (7.21). **FT−IR** (ATR, $\tilde{\nu}_{max}/cm^{-1}$): 3066 (w, C-$H_{ar}$), 2952, 2899, 2864 (w, C-H_{alif}), 1598,1567 (m, C-C_{ar} a C_{ar}-N). **UV – VIS** (acetonitrile, λ/nm, 1.10^{-5} mol·L^{-1}): 315 (π → π*), 338 (n → π*).

Crystallography

Data collection and cell refinement of **1**–**4** were made by Stoe StadiVari diffractometer at 100 K using Pilatus3R 300K HPAD detector and microfocused source Xenocs Genix3D Cu HF (Cu Kα radiation λ = 1.54186 Å). The diffraction intensities were corrected for Lorentz and polarization factors. The structures were solved using SUPERFLIP[1] or SHELXT[2] program and refined by full-matrix least-squares procedure with SHELXL (version 2018/3).[3] The multi-scan absorption corrections were applied using Stoe LANA software.[4] Geometrical analyses were performed with SHELXL. The structures were drawn with MERCURY.[5]

Magnetic measurements

Herein reported magnetic investigation have been carried out on MPMS XL-7 SQUID or MPMS XL-5 SQUID magnetometer (Quantum design Inc., San Diego, CA, USA). The gelatine capsules were used as sample holders and their small diamagnetic contribution is negligible in the overall magnetization, which was dominated by the sample. In the case of magnetic experiments at static magnetic field (DC), the temperature-dependency was recorded in the thermal range 1.9 – 300 K at B = 0.1 T using the 1 K/min sweeping rate, and field-dependency was measured at isothermal conditions in the range B = 0 – 7 T. Collected data were corrected for the diamagnetism using the Pascal constants[6] and transformed into the μ_{eff} vs T and M_{mol} vs B dependencies. The experimental details about the magnetic experiments at AC magnetic field are given in the S4 section (*vide infra*).

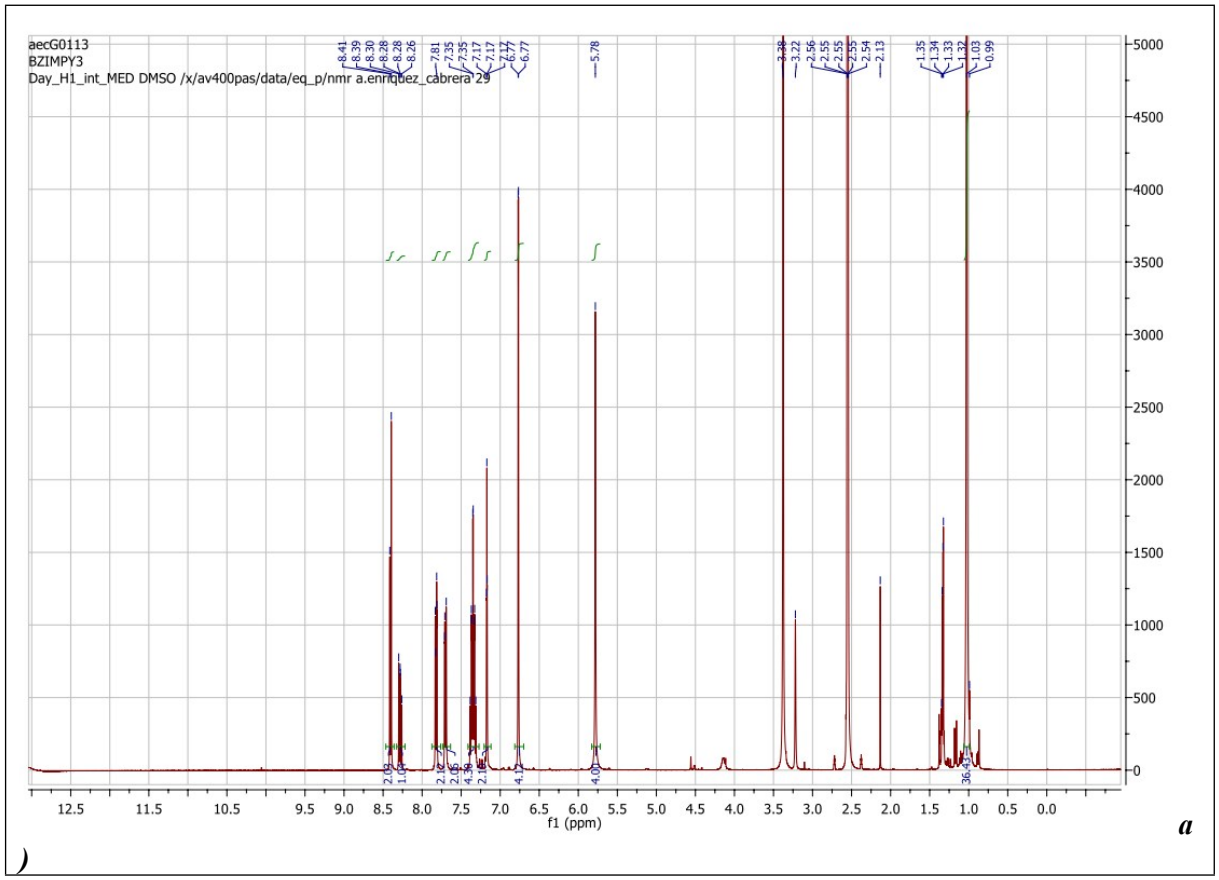

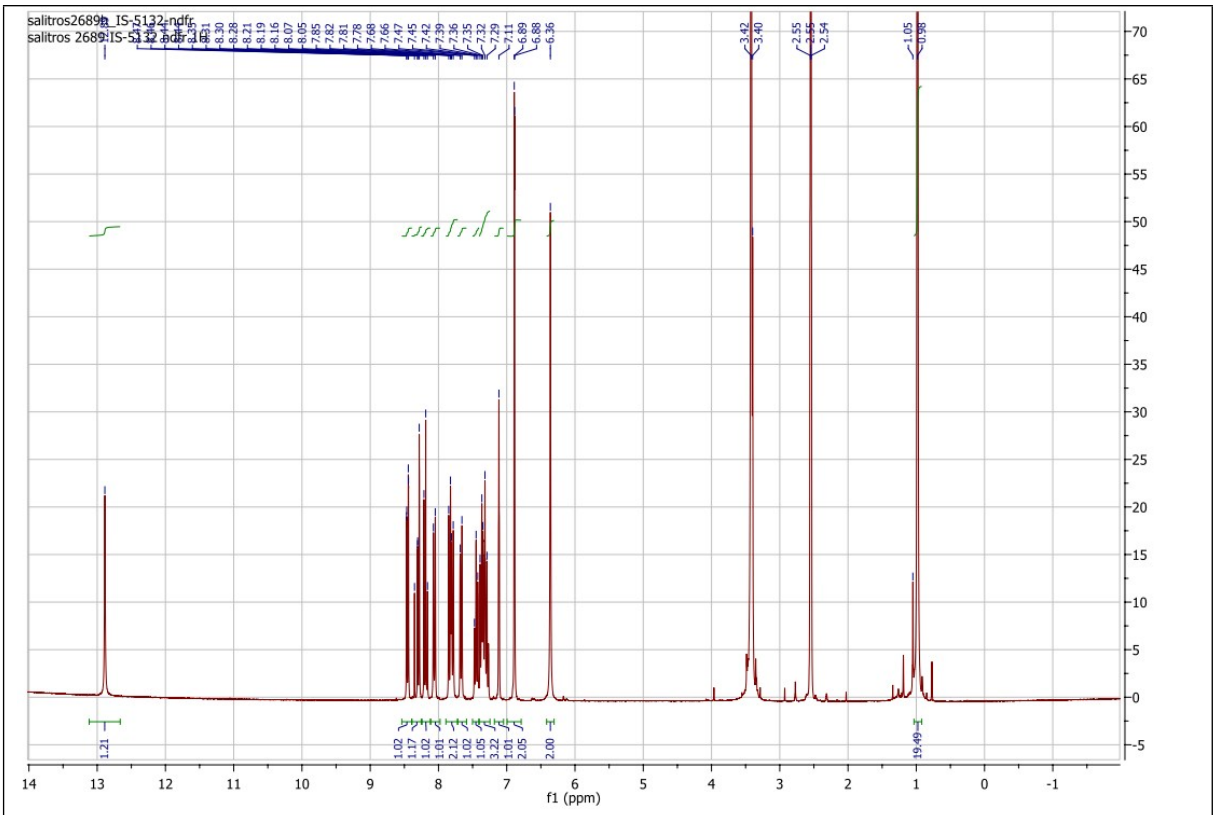
salitros2689a_IS-5132-ndfr
salitros 2689-IS-5132-5dfr-1H
f1 (ppm)

b)

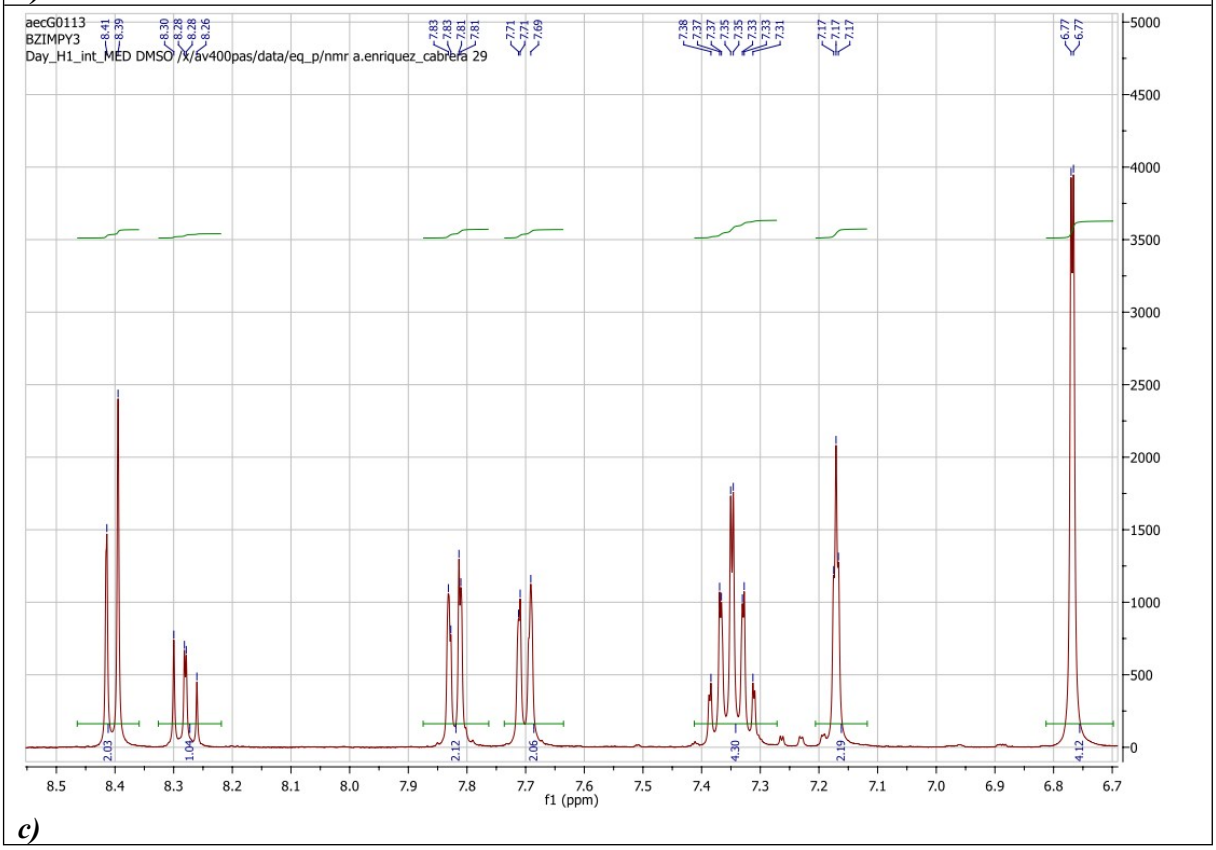
aecG0113
BZIMPY3
Day_H1_int_MED DMSO /x/av400pas/data/eq_p/nmr a.enriquez_cabrera 29
f1 (ppm)

c)

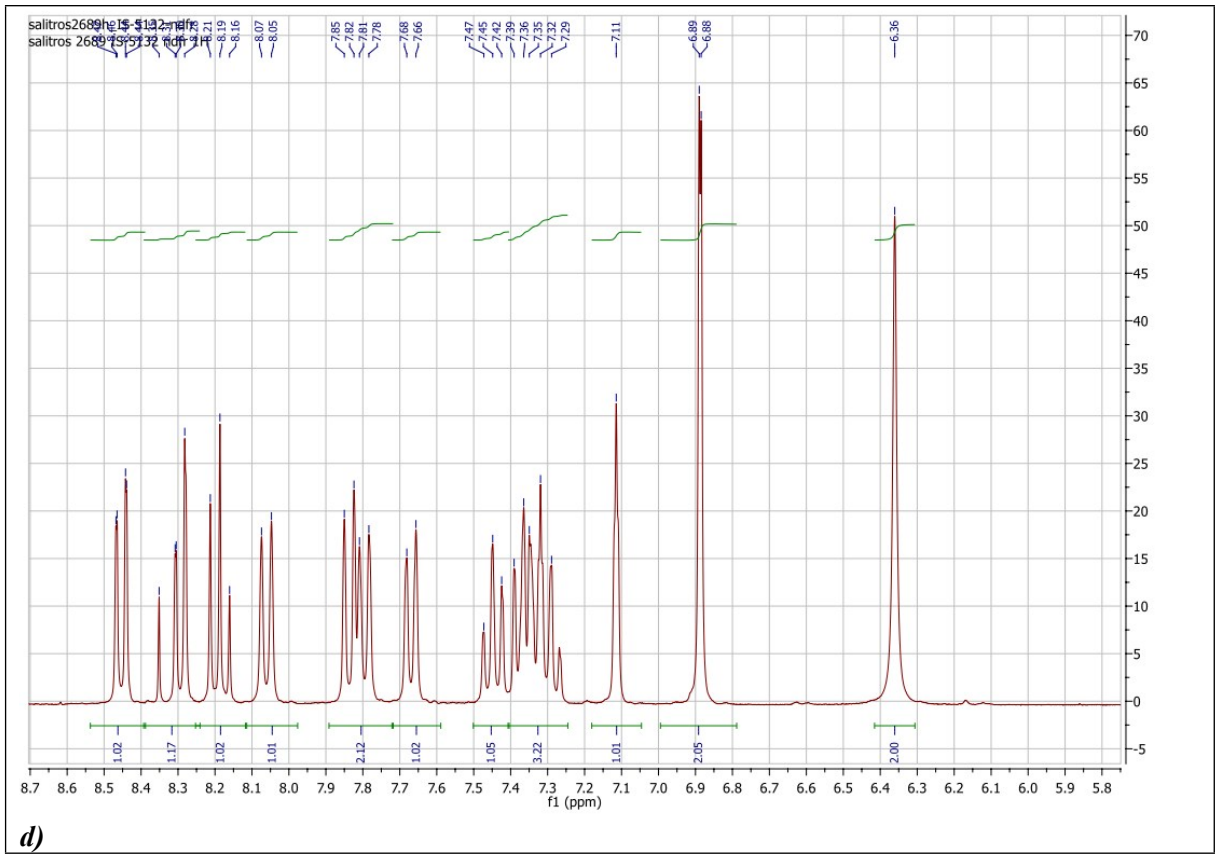

d)

Figure S1.1 [1]H NMR spectrum of ligand L (a) and L1 (b) and zoomed aromatic region of ligand L (***c***) and ligand L1(***d***)

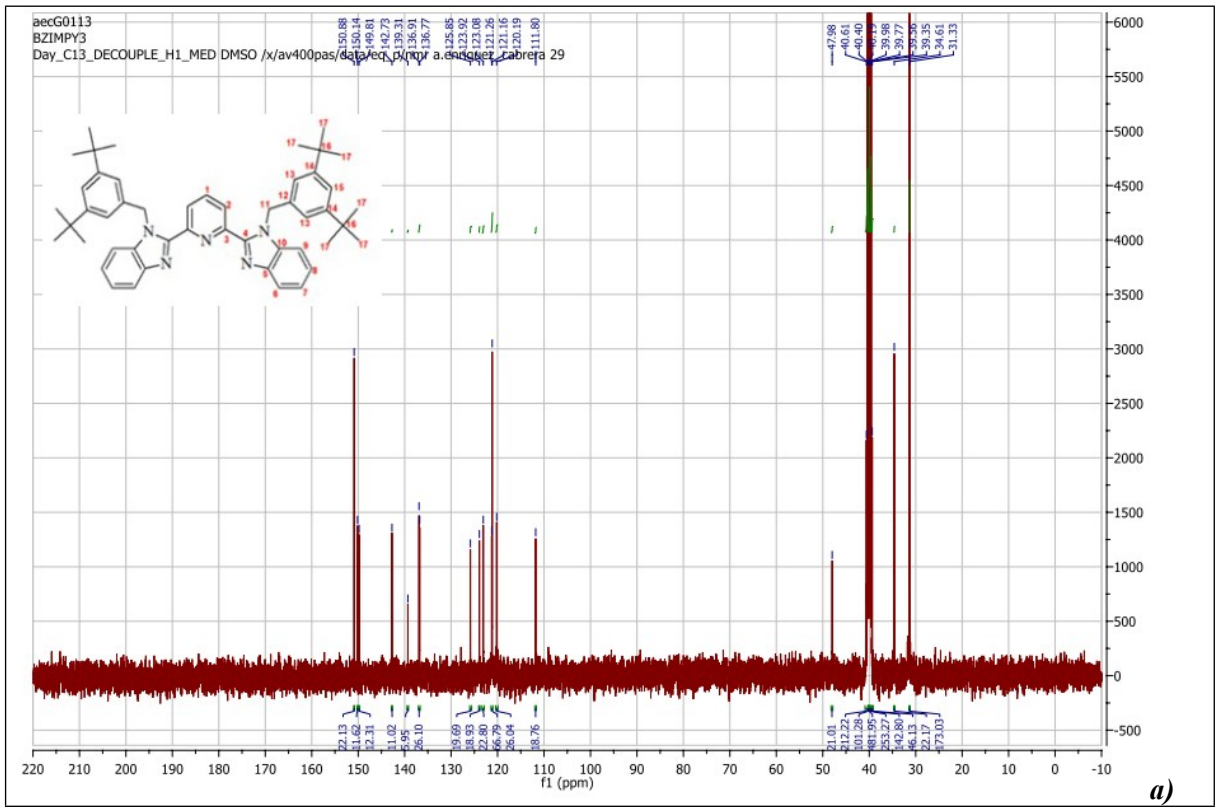

a)

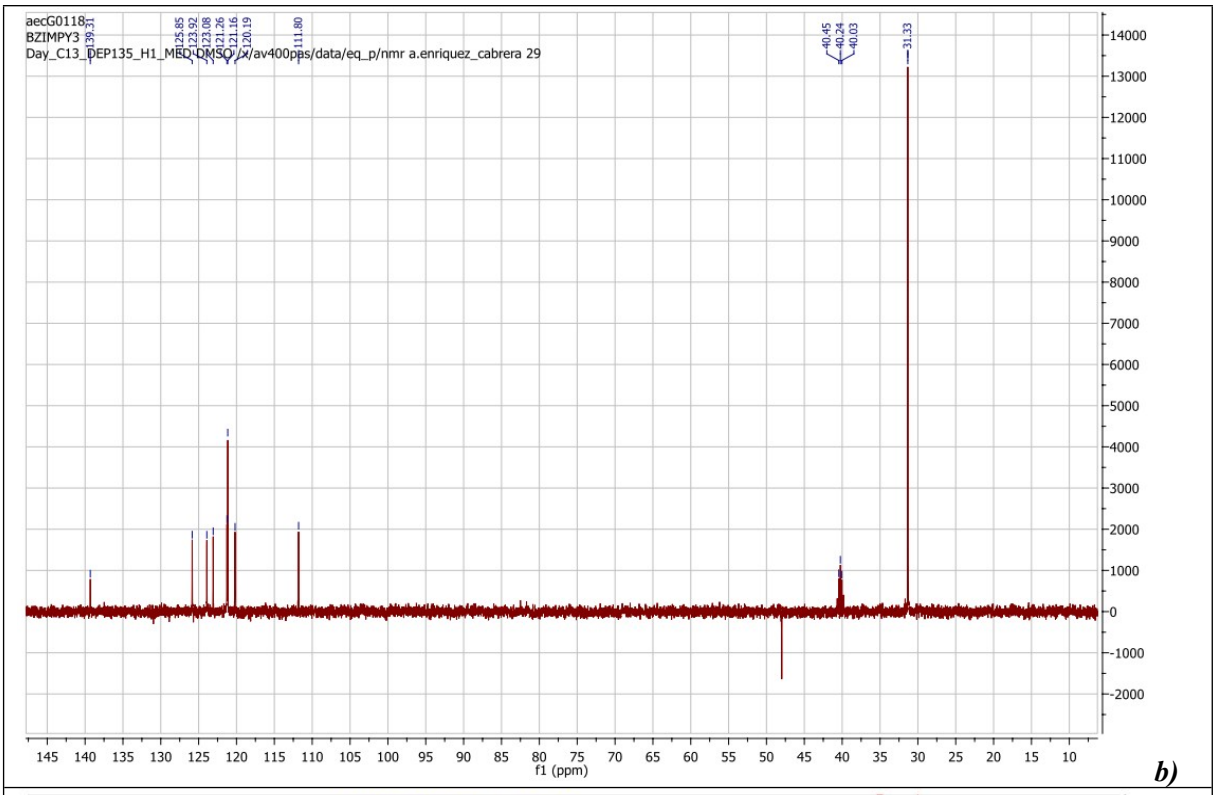
aecG0118
BZIMPY3
Day_C13_DEP135_H1_MEO_DMSO_/x/av400pas/data/eq_p/nmr a.enriquez_cabrera 29
139.37
125.65
123.92
123.08
121.76
121.16
120.19
111.80
40.45
40.24
40.03
31.33
f1 (ppm)

b)

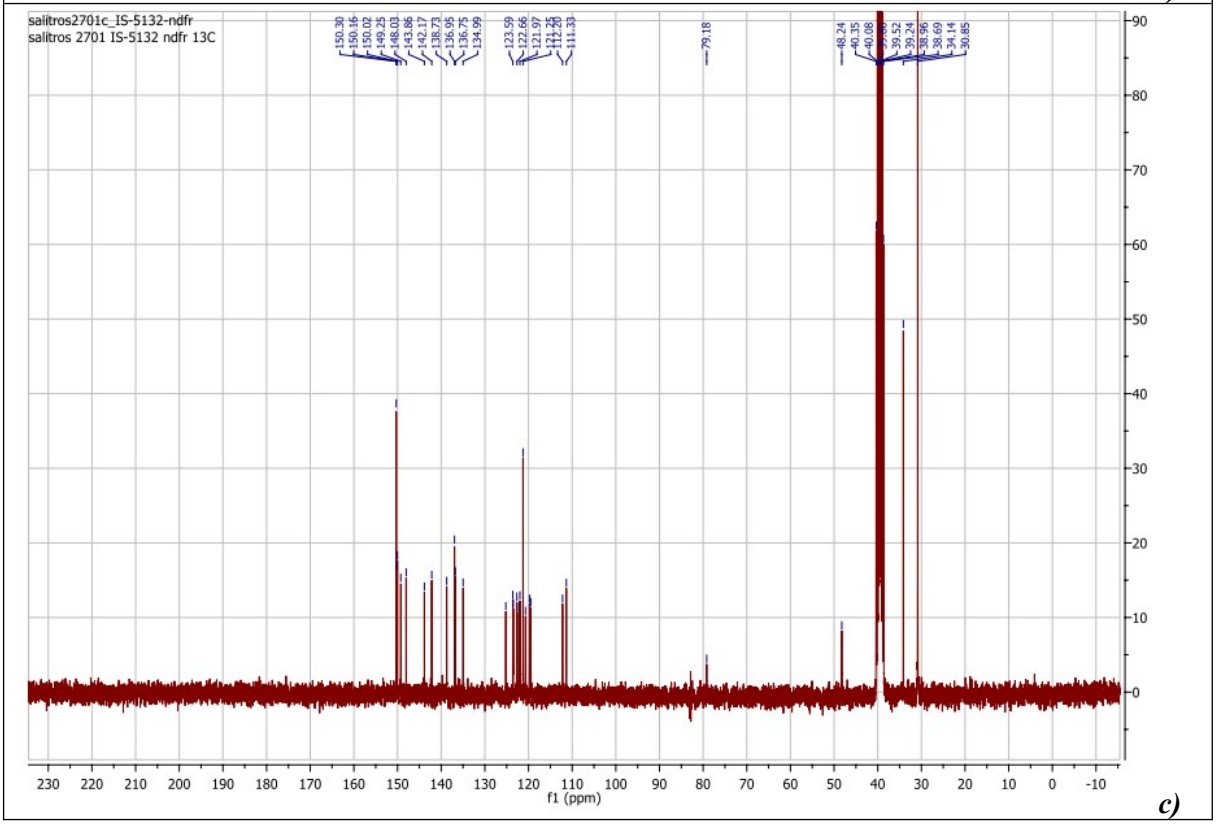
salitros2701c_IS-5132-ndfr
salitros 2701 IS-5132 ndfr 13C
150.30
150.16
150.02
149.25
148.03
143.86
142.17
138.73
136.95
136.75
134.99
123.59
122.66
121.97
112.20
111.33
79.18
48.24
40.35
40.08
39.52
39.24
38.96
38.69
34.14
30.85
f1 (ppm)

c)

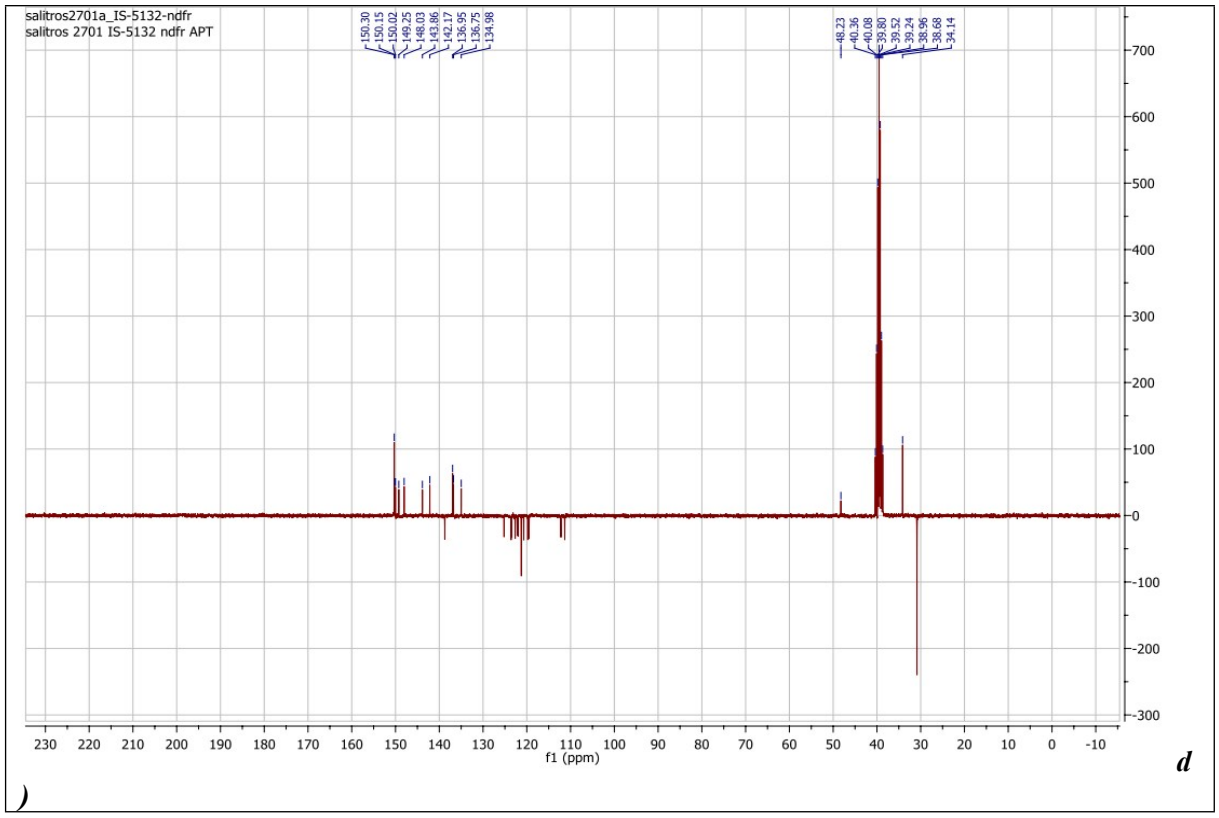

Figure S1.2 ^{13}C NMR (***a***) and APT (***b***) spectra of ligand L. ^{13}C NMR (***c***) and APT (***d***) spectra of ligand L1.

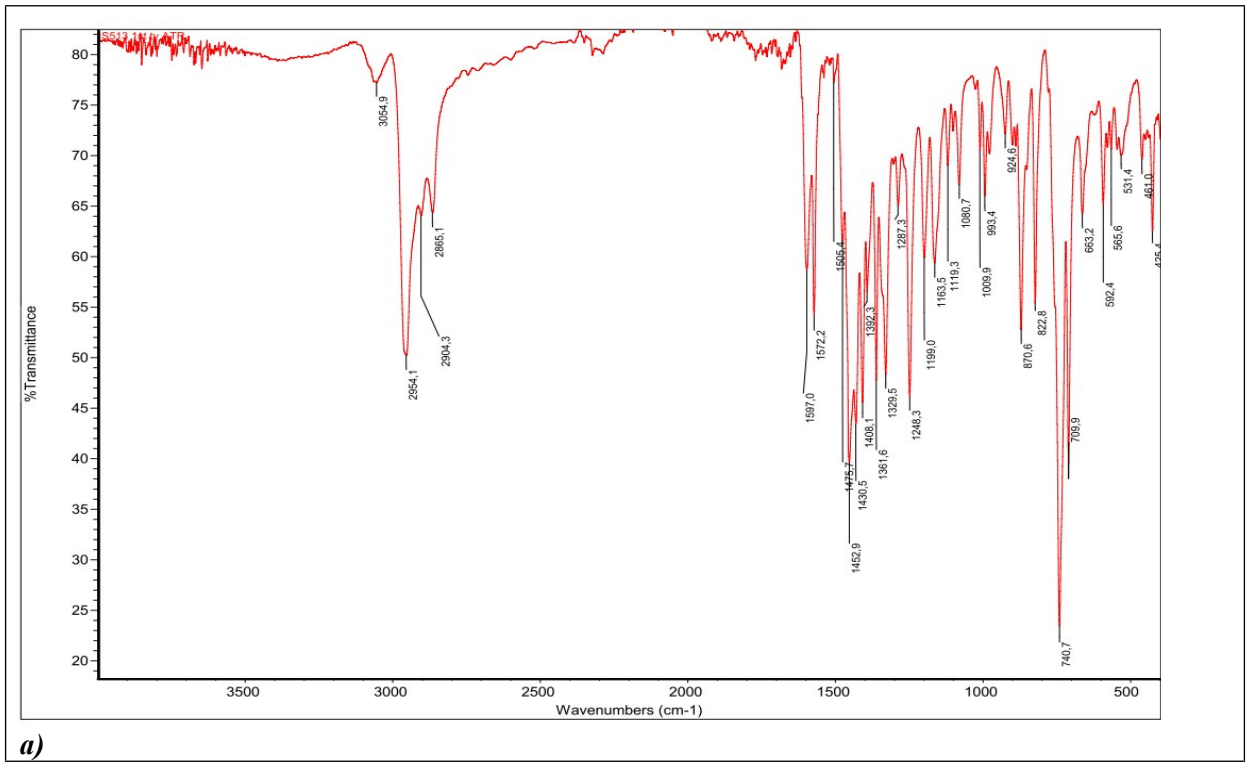

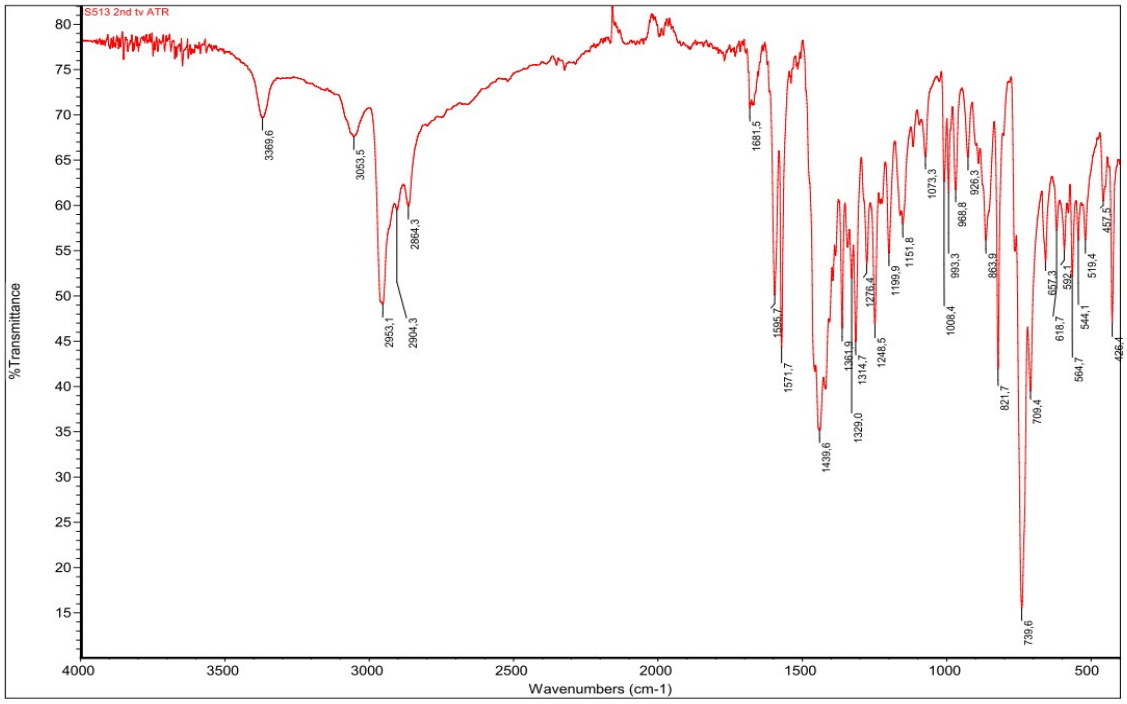
S513 2nd tv ATR
%Transmittance
Wavenumbers (cm-1)
4000
3500
3000
2500
2000
1500
1000
500
3369.6
3053.5
2953.1
2904.3
2864.3
1681.5
1571.7
1439.6
1329.0
1199.9
1151.8
1073.3
1008.4
993.3
968.8
926.3
863.9
821.7
739.6
709.4
657.3
618.7
592.1
564.7
544.1
519.4
457.5

b)

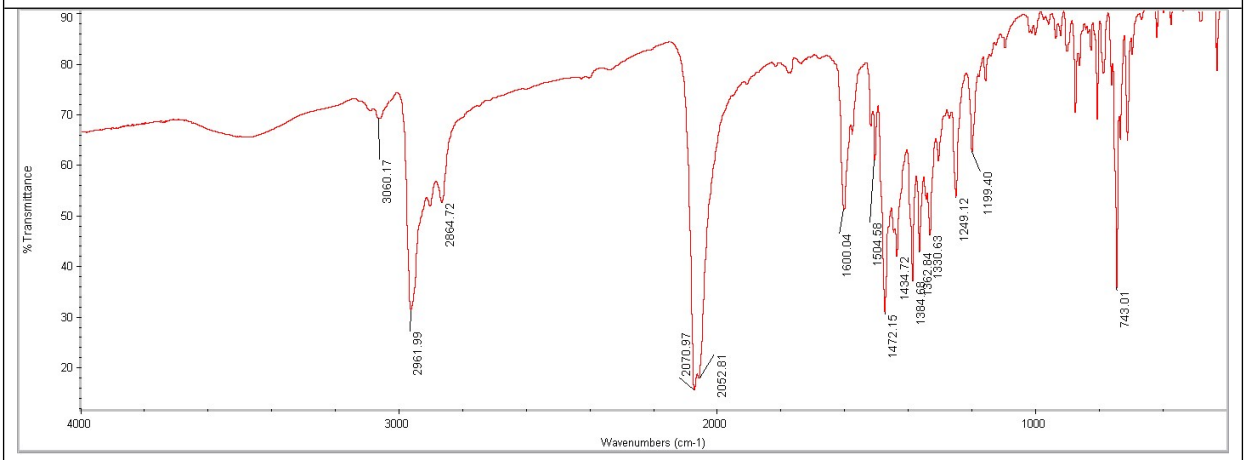
% Transmittance
Wavenumbers (cm-1)
4000
3000
2000
1000
3060.17
2961.99
2864.72
2070.97
2052.81
1600.04
1504.58
1472.15
1434.72
1384.68
1362.84
1330.63
1249.12
1199.40
743.01

c)

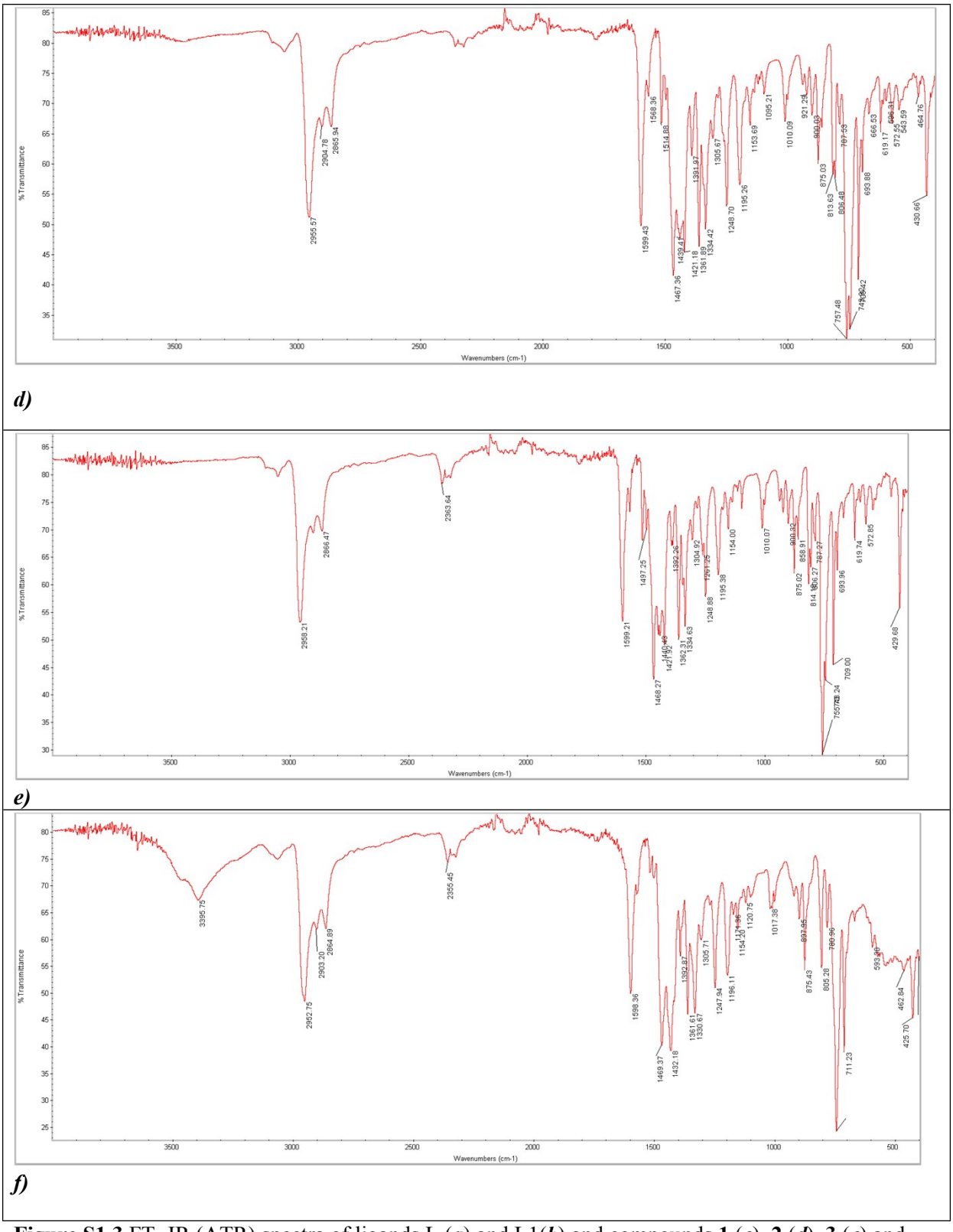

d)

e)

f)

Figure S1.3 FT−IR (ATR) spectra of ligands L (***a***) and L1(***b***) and compounds **1** (***c***), **2** (***d***), **3** (***e***) and **4**(***f***).

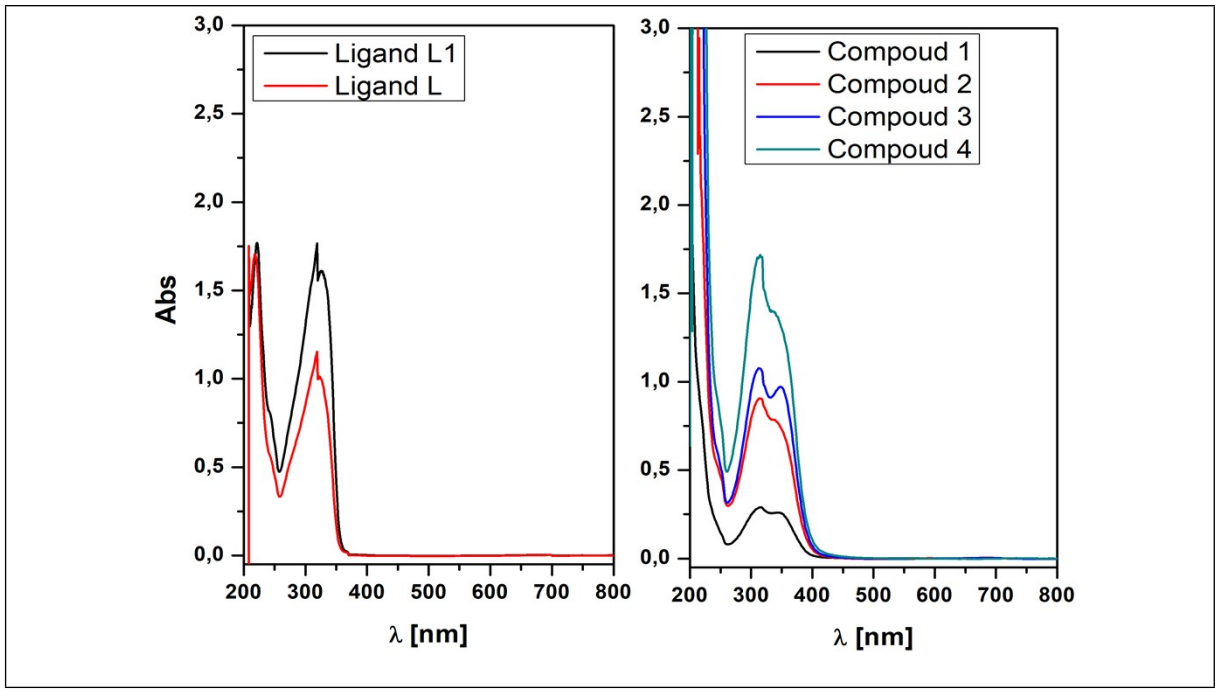

Figure S1.4 UV−VIS acetonitrile solution spectra of ligands L and L1 (***left)*** and compounds **1** – **4** (***right***).

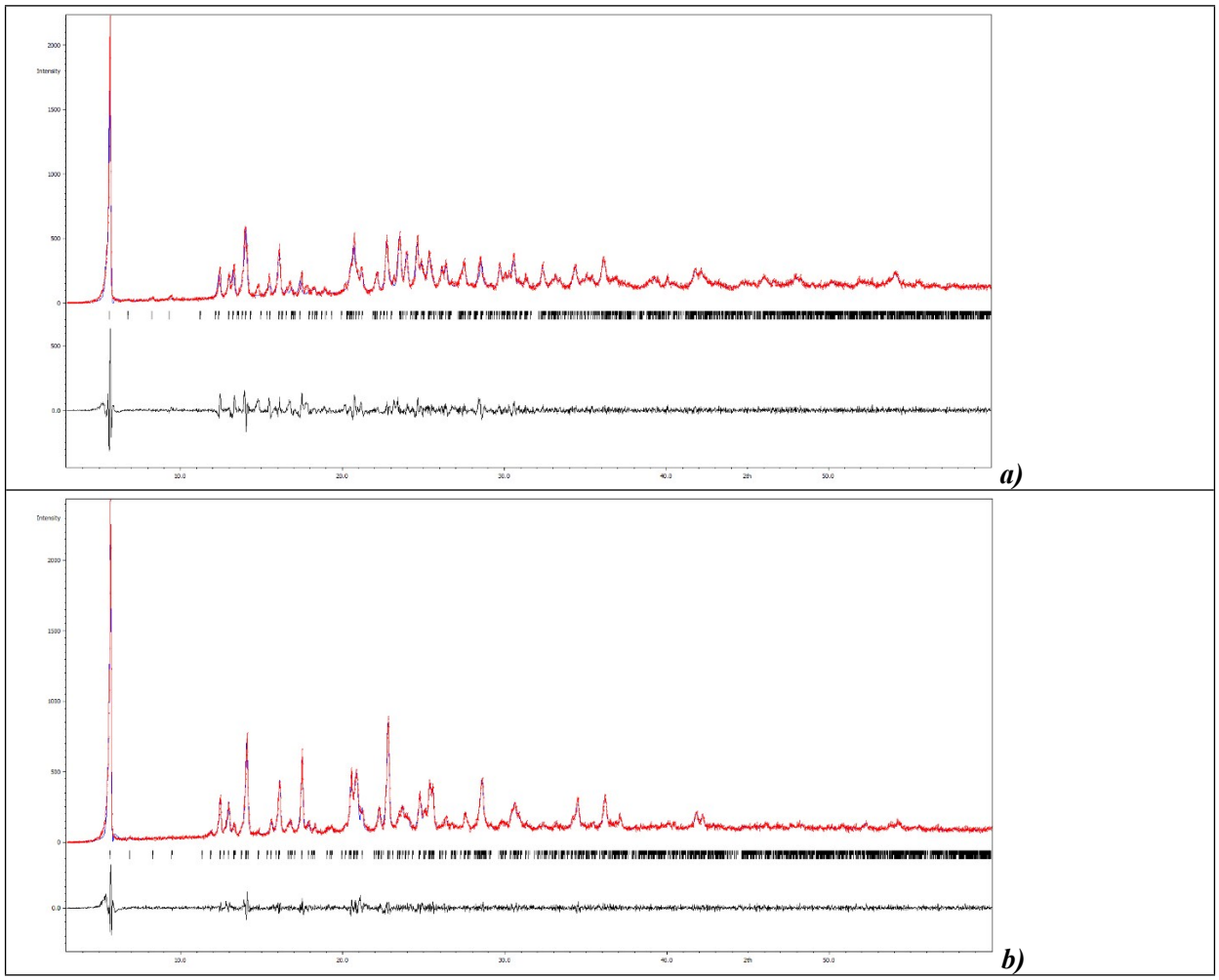

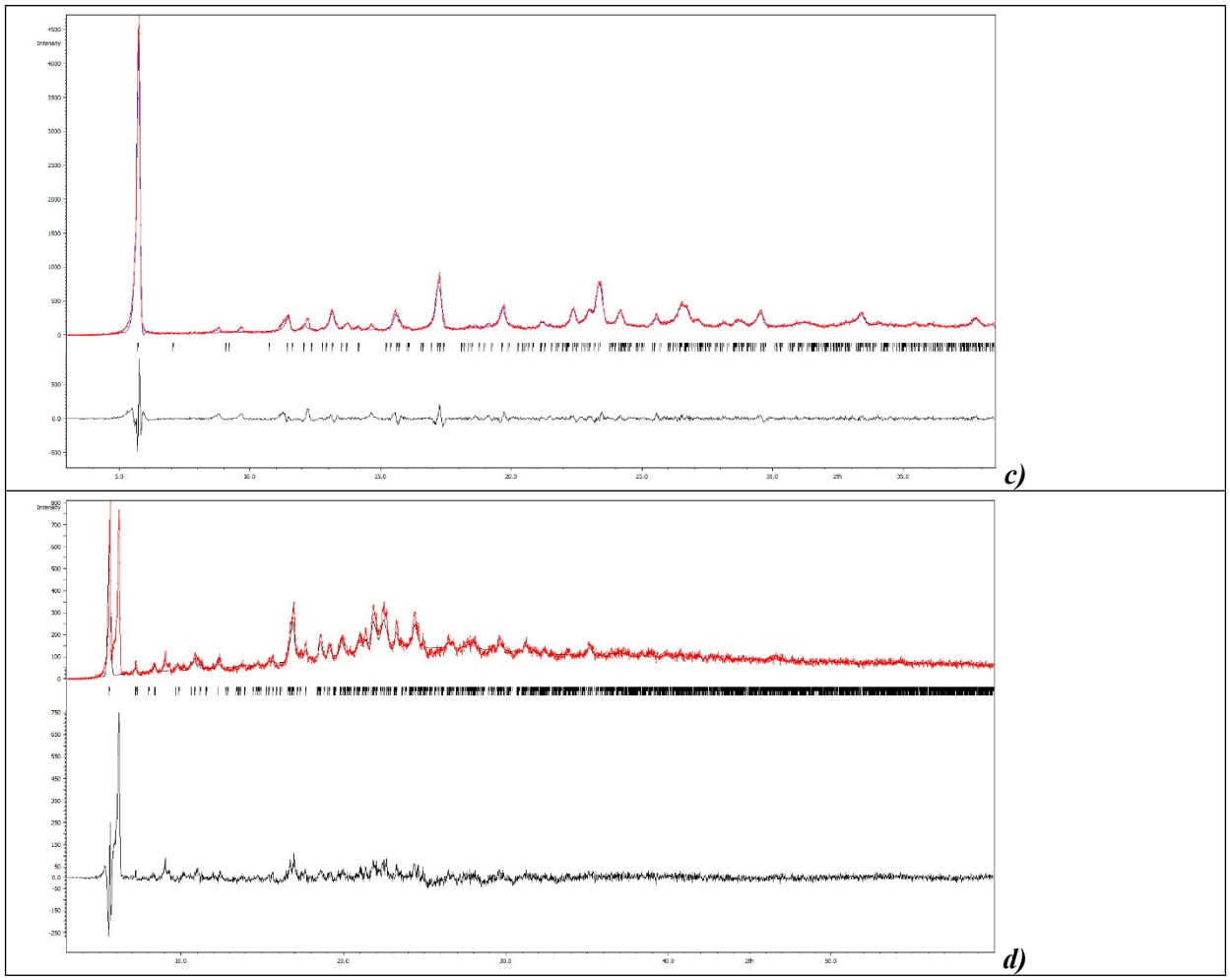

Figure S1.5 X-ray powder diffractograms of **1**(***a***), **2**(***b***) and **3**(***c***). The red and blue lines present experimental and simulated diffractions, respectively. The black lines present subtracted differences between the measured and simulated spectra. Diffractions of **4** (***d***, red line) are compared with Zn(II) hexacoordinated analogue ($[Zn(L)_2](Br)_2$) and subtraction of both spectra (black line in the bottom part of graph) indicates different symmetries of both complexes.

S2 Structural Information

Table S2.1 Results of the SHAPE calculations for coordination polyhedra **1-3**. PP (D_{5h}) – pentagon; vOC (C_{4v}) vacant octahedron; TBPY (D_{3h}) trigonal bipyramid; SPY (C_{4v}) spherical square pyramid; JTBPY (D_{3h}) Johnson trigonal bipyramid

	1	**2**	**3**
PP (D_{5h})	31.714	33.859	36.077
vOC (C_{4v})	2.134	8.040	8.289
TBPY (D_{3h})	5.502	**1.988**	**2.520**
SPY (C_{4v})	**1.366**	4.869	4.871
JTBPY (D_{3h})	7.864	6.195	7.401
τ_5	0.30	0.5	0.41

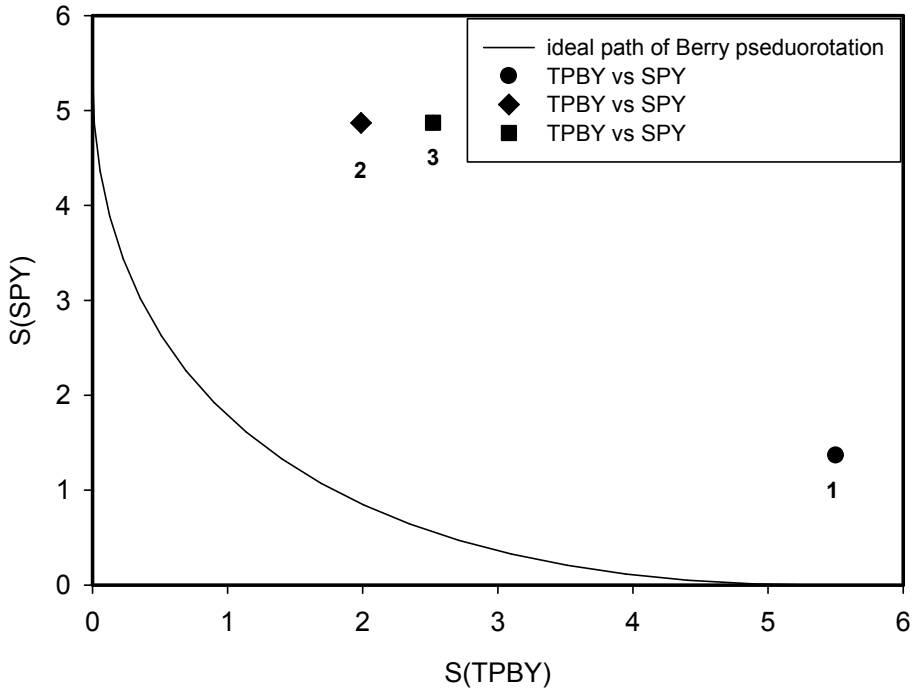

Figure S2.1 Shape map of coordination polyhedra in **1-3**. Solid line represents Berry pseudorotation from between square pyramidal (SPY-5) and trigonal bipyramidal (TBPY-5) geometry.

a)

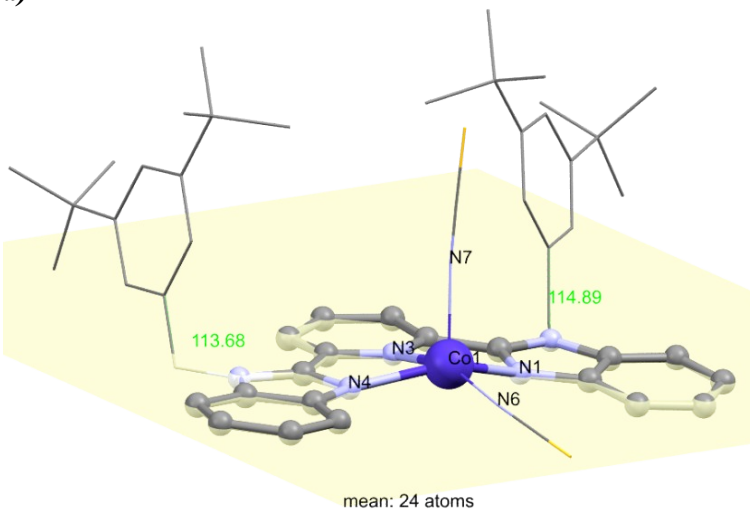

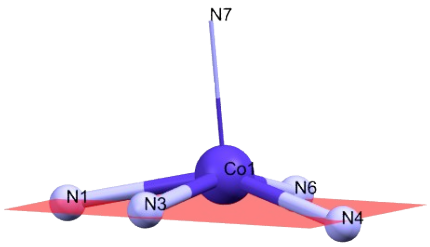

Axial angles: N7-Co1-N1=97.93(8)°; N7-Co1-N3=89.36(8)°; N7-Co1-N4=102.76(8)°; N7-Co1-N6= 109.86(9)°. Equatorial angles: N3-Co1-N4=74.73(7)°; N4-Co1-N6=100.97(8)°; N6-Co1-N1=100.55(8)°; N1-Co1-N3=74.96(7)°, N4-Co1-N1=142.80(8); N3-Co1-N6= 160.76(8)°.

b)

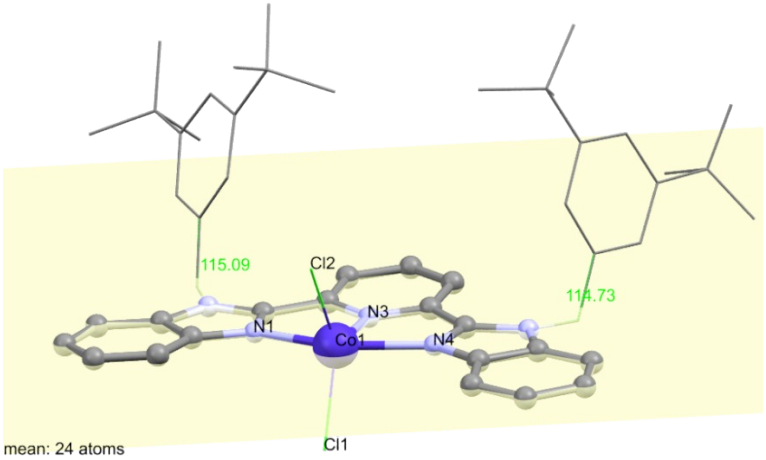

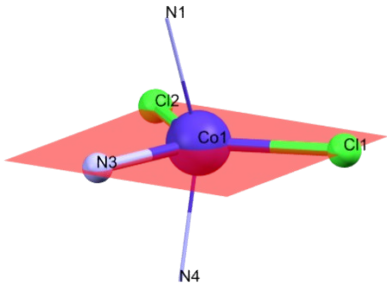

Axial angle: N1-Co1-N4=151.33(8)°.
Equatorial angles: Cl1-Co1-Cl2=123.47(3)°; Cl2-Co1-N3=116.55(6)°; N3-Co1-Cl1=119.96(6)°.

c)

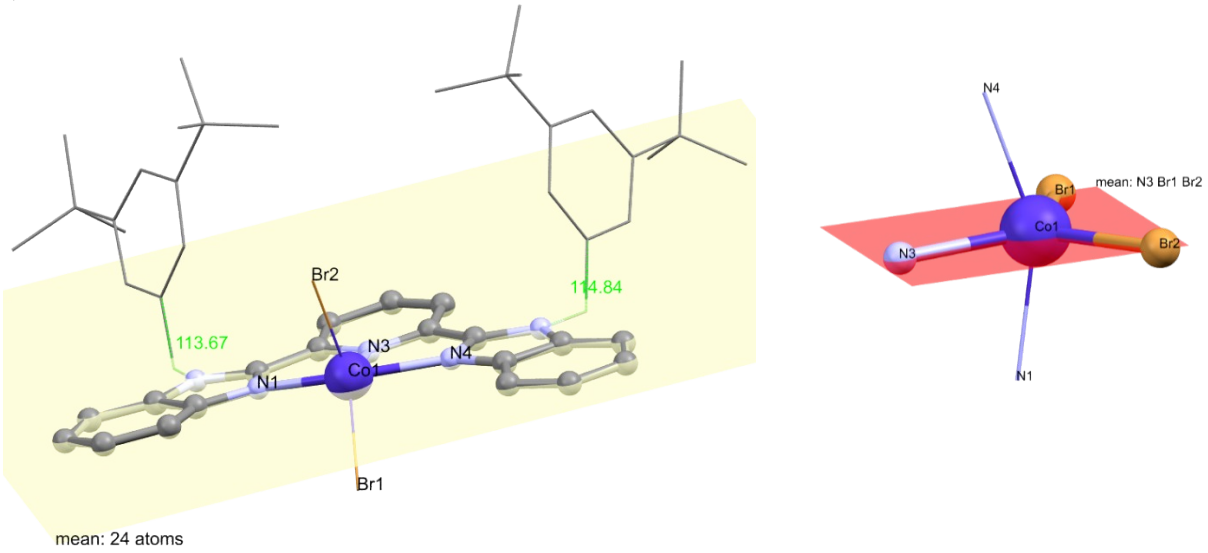

Axial angle: N1-Co1-N4=152.0(1)°.
Equatorial angles: Br1-Co1-Br2=127.47(3)°; Br2-Co1-N3=110.77(8)°; N3-Co1-Br1=121.71(8)°.

Figure S2.2 Visualization of the Co(II) central atom position with respect to the plane of aromatic chelating ligand L (left) and with respect to equatorial or square planar planes in the complex **1** (***a***), **2** (***b***) and **3** (***c***).

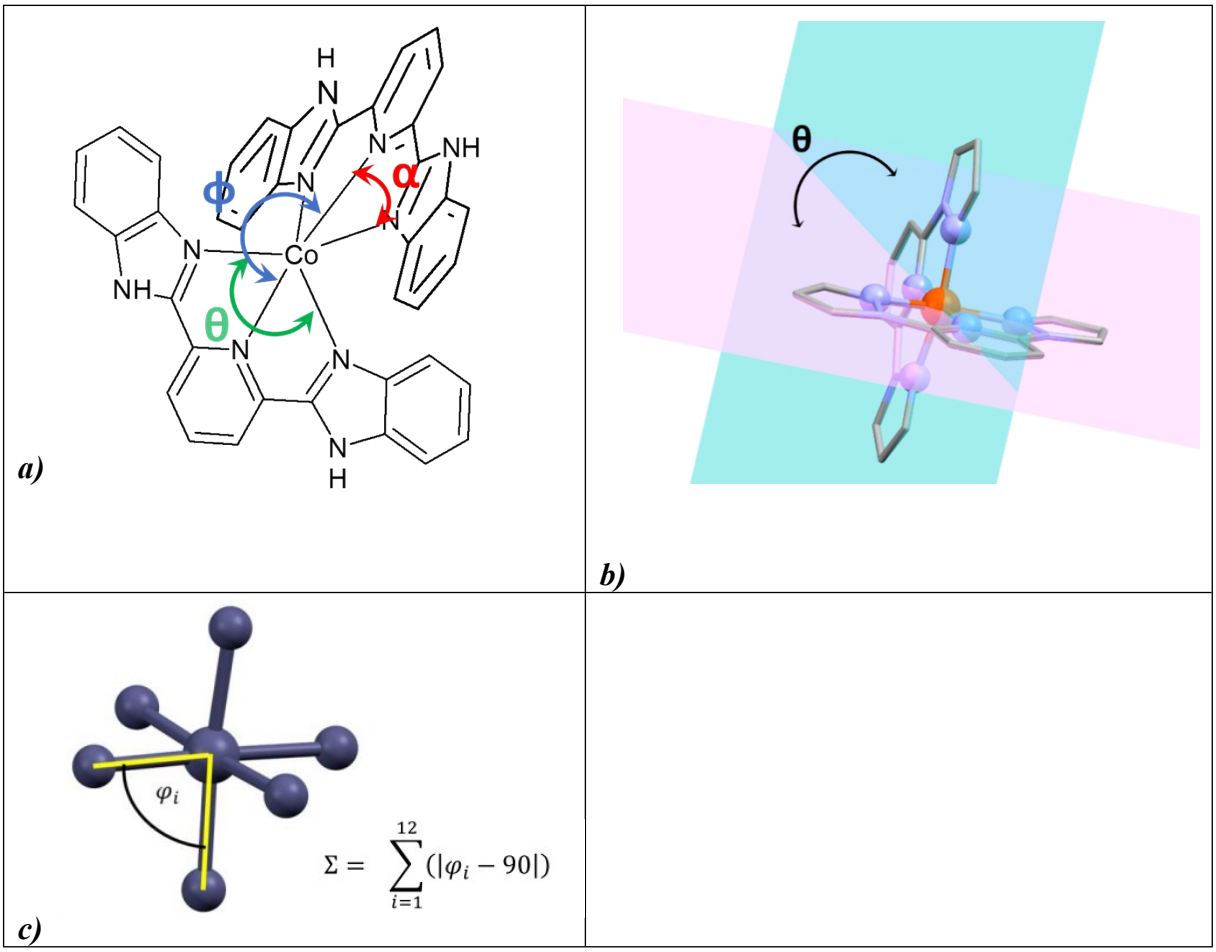

Figure S2.3 Schematic representation of the angular metric parameter. ***a)*** α – bite angle (average value of four N_{im}-Co-N_{py}); ϕ – *trans* angle N_{py}-Co-N_{py}; φ- clamp angle (average value of two N_{pz}-Fe-N_{pz}) ***b)*** θ - dihedral angle between the least squares planes of the two *bpp* moieties coordinating the same metal center[7] ***c)*** Distortion parameters $\mathbf{\Sigma}$; φ_i is one of 12 octahedron *cis* angles utilized in calculation of $\mathbf{\Sigma}$ parameter.[8]

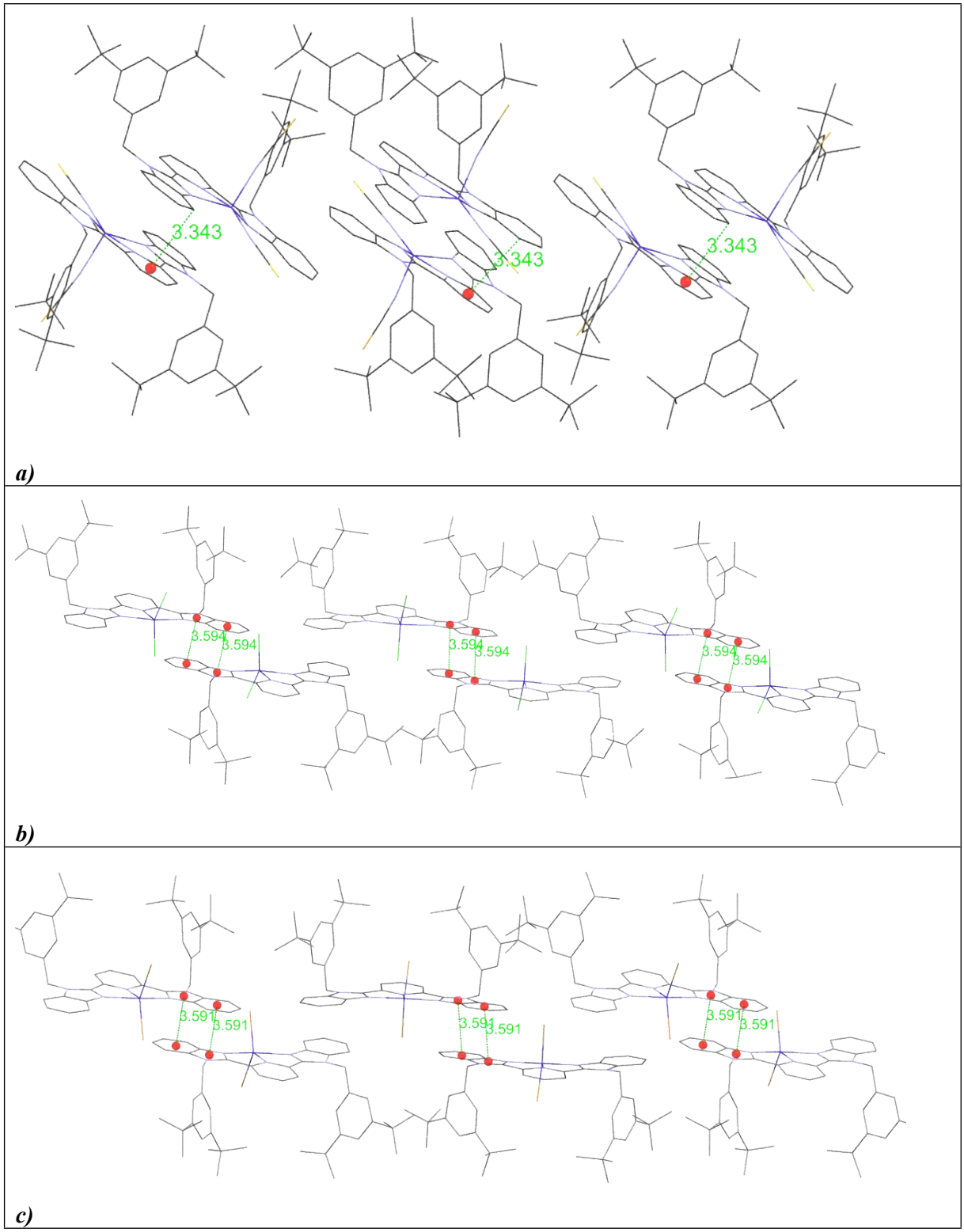

Figure S2.4 Visualization of non-covalent supramolecular interactions in the crystal structure of **1** (***a***), **2** (***b***) and **3** (***c***).

S3 Computational detials

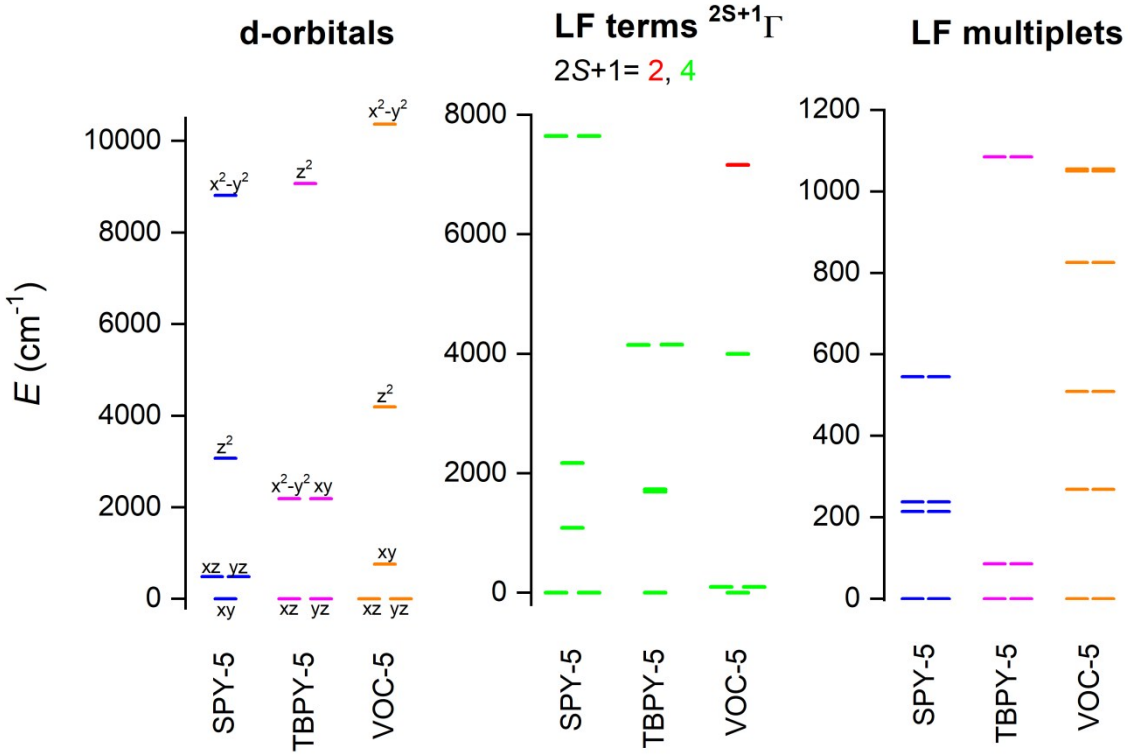

Figure S3.1 The graphical output of the CASSCF/NEVPT2 calculations with CAS(7,5) for the model compound $[CoCl_5]^{3-}$ with ideal geometries defined by program SHAPE, where SPY is square pyramid, TBPY is trigonal bipyramid and vOC is vacant octahedron. Plot of the d-orbitals splitting calculated by *ab initio* ligand field theory (AILFT) (*left*), low-lying ligand-field terms (*middle*), and ligand-field multiplets – Kramers doublets (*right*). The doublet and quartet spin states are shown in red and green, respectively.

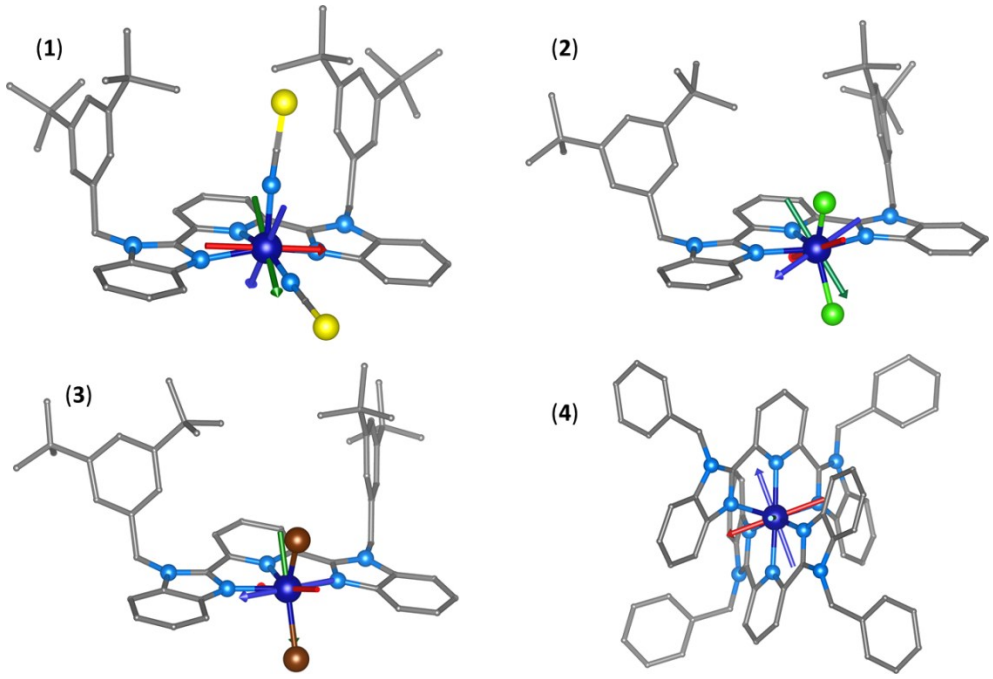

Figure S3.2 Representation of the molecular fragments of **1-4** derived from the experimental X-ray geometry used for CASSCF/NEVPT2's calculation with CAS(7,5), also showing the principal axes of the *D*-tensor with the arrows (x-axis is red, y-axis is green, and z-axis is blue).

Table S3.1 Individual contributions to *D*-tensor obtained from the calculation based on CASSCF/NEVPT2 with CAS(7,5) for the mononuclear molecular fragments of **1-4**.

[Co(L)(NCS)$_2$] of **1**					[Co(L)Cl$_2$] of **2**					[Co(L)Br$_2$] of **3**					[Co(L')$_2$]$^{2+}$ of **4**				
Block	Mult	Root	D	E	Block	Mult	Root	D	E	Block	Mult	Root	D	E	Block	Mult	Root	D	E
0	4	0	-0.000	-0.000	0	4	0	-0.000	-0.000	0	4	0	-0.000	0.000	0	4	0	0.000	0.000
0	4	1	26.815	26.720	0	4	1	8.556	8.616	0	4	1	16.696	16.675	0	4	1	28.786	27.549
0	4	2	12.840	-12.762	0	4	2	1.256	-1.741	0	4	2	-0.298	-3.277	0	4	2	20.154	-19.424
0	4	3	3.415	-3.338	0	4	3	18.173	-16.370	0	4	3	12.374	-7.474	0	4	3	2.479	1.963
0	4	4	-12.670	0.001	0	4	4	17.448	15.494	0	4	4	15.497	7.315	0	4	4	-0.301	-0.475
0	4	5	0.867	-0.860	0	4	5	0.017	0.012	0	4	5	0.200	0.074	0	4	5	0.450	-0.453
0	4	6	-0.417	0.026	0	4	6	0.002	-0.003	0	4	6	0.020	-0.019	0	4	6	0.000	0.001
0	4	7	0.003	-0.003	0	4	7	0.002	-0.001	0	4	7	0.002	0.000	0	4	7	0.106	-0.082
0	4	8	-0.065	0.020	0	4	8	0.122	-0.121	0	4	8	0.119	-0.124	0	4	8	0.009	0.009
0	4	9	0.039	-0.038	0	4	9	0.122	0.121	0	4	9	0.112	0.111	0	4	9	0.084	0.064
1	2	0	-0.511	-1.555	1	2	0	0.036	0.013	1	2	0	-0.172	0.079	1	2	0	-0.550	-0.387
1	2	1	-0.206	0.190	1	2	1	-0.003	-0.004	1	2	1	0.000	-0.023	1	2	1	6.123	1.329
1	2	2	-0.236	-0.895	1	2	2	4.459	-0.004	1	2	2	4.574	0.255	1	2	2	-0.013	0.005
1	2	3	-0.399	-0.449	1	2	3	-0.174	-0.174	1	2	3	-1.273	-1.242	1	2	3	-0.018	-0.016
1	2	4	-0.030	0.030	1	2	4	-1.243	-1.245	1	2	4	-1.074	1.067	1	2	4	-0.986	-0.964
1	2	5	-0.004	0.006	1	2	5	-0.537	0.548	1	2	5	-0.190	0.021	1	2	5	-1.042	0.921
1	2	6	-1.259	-1.450	1	2	6	-0.440	-0.237	1	2	6	-0.359	0.435	1	2	6	-0.447	-0.016
1	2	7	-1.843	1.840	1	2	7	-1.137	1.073	1	2	7	-0.520	-0.470	1	2	7	-0.065	-0.039
1	2	8	2.445	-0.374	1	2	8	7.671	0.000	1	2	8	5.586	0.008	1	2	8	3.634	-0.001
1	2	9	0.069	0.005	1	2	9	-0.005	0.006	1	2	9	0.024	-0.002	1	2	9	-0.021	-0.020
1	2	10	-0.312	0.300	1	2	10	0.002	-0.003	1	2	10	-0.006	-0.011	1	2	10	-0.013	0.022
1	2	11	-0.012	0.012	1	2	11	-0.000	0.000	1	2	11	-0.001	-0.001	1	2	11	-0.037	-0.027
1	2	12	-0.051	0.052	1	2	12	-0.010	0.009	1	2	12	-0.045	0.038	1	2	12	-0.049	0.190
1	2	13	-0.229	-0.230	1	2	13	-0.059	-0.058	1	2	13	-0.062	-0.062	1	2	13	-0.346	-0.266
1	2	14	-0.361	0.362	1	2	14	-0.002	-0.002	1	2	14	0.003	-0.004	1	2	14	-0.119	0.092
1	2	15	-0.045	0.045	1	2	15	0.050	0.001	1	2	15	0.050	0.020	1	2	15	-0.103	0.080
1	2	16	-0.041	-0.040	1	2	16	-0.132	-0.139	1	2	16	-0.094	-0.013	1	2	16	-0.074	-0.005
1	2	17	-0.051	-0.224	1	2	17	-0.082	0.081	1	2	17	-0.025	-0.010	1	2	17	-0.050	-0.047
1	2	18	-0.167	0.162	1	2	18	-0.040	0.040	1	2	18	-0.060	-0.016	1	2	18	0.855	0.330
1	2	19	-0.019	-0.158	1	2	19	0.261	-0.007	1	2	19	0.174	0.056	1	2	19	-0.147	-0.114
1	2	20	2.551	-0.054	1	2	20	-0.012	0.012	1	2	20	0.033	0.006	1	2	20	0.356	0.032
1	2	21	-0.185	0.207	1	2	21	0.087	-0.046	1	2	21	0.729	0.074	1	2	21	-0.277	-0.288
1	2	22	-0.029	-0.027	1	2	22	-0.024	0.025	1	2	22	-0.086	-0.013	1	2	22	-0.208	0.182
1	2	23	-0.088	-0.116	1	2	23	1.284	-0.001	1	2	23	-0.108	-0.115	1	2	23	0.161	0.075
1	2	24	-0.131	0.130	1	2	24	0.156	0.005	1	2	24	0.029	0.002	1	2	24	-0.010	-0.007
1	2	25	-0.012	-0.100	1	2	25	-0.005	-0.011	1	2	25	0.423	0.013	1	2	25	-0.138	0.031
1	2	26	-0.001	0.001	1	2	26	-0.784	0.786	1	2	26	-0.522	0.339	1	2	26	-0.161	-0.036
1	2	27	0.025	-0.005	1	2	27	-0.668	-0.667	1	2	27	-0.654	-0.275	1	2	27	-0.026	-0.027
1	2	28	-0.176	0.171	1	2	28	-0.297	-0.149	1	2	28	-0.258	0.040	1	2	28	0.019	0.018
1	2	29	-0.003	0.002	1	2	29	-0.299	0.147	1	2	29	-0.289	-0.083	1	2	29	-0.066	-0.054
1	2	30	0.081	-0.082	1	2	30	-0.006	0.005	1	2	30	-0.001	0.001	1	2	30	-0.018	-0.012
1	2	31	0.022	-0.048	1	2	31	-0.026	-0.025	1	2	31	-0.016	-0.001	1	2	31	-0.032	-0.021
1	2	32	-0.006	0.005	1	2	32	0.001	-0.001	1	2	32	0.009	0.005	1	2	32	-0.024	-0.016
1	2	33	-0.026	0.026	1	2	33	-0.001	0.001	1	2	33	-0.001	-0.000	1	2	33	-0.063	0.043
1	2	34	-0.004	-0.006	1	2	34	0.000	-0.001	1	2	34	-0.000	-0.000	1	2	34	0.000	-0.000
1	2	35	0.014	-0.015	1	2	35	0.133	-0.002	1	2	35	0.123	0.006	1	2	35	0.068	0.013
1	2	36	-0.000	-0.000	1	2	36	0.038	-0.002	1	2	36	-0.002	-0.004	1	2	36	0.000	-0.000
1	2	37	-0.011	-0.014	1	2	37	-0.005	0.006	1	2	37	-0.002	0.004	1	2	37	-0.007	-0.004
1	2	38	-0.010	0.010	1	2	38	0.001	0.000	1	2	38	-0.002	-0.002	1	2	38	0.018	0.007
1	2	39	-0.007	-0.020	1	2	39	0.002	-0.000	1	2	39	-0.000	0.002	1	2	39	0.019	0.000

S4 AC Susceptibility Measurements

The mapping of the magnetic susceptibility components as functions of the applied external DC field for a set of four frequencies of the AC field at $T = 2.0$ K is shown in Figure S4.1.

Compound **1**	Compound **2**	Compound **3**

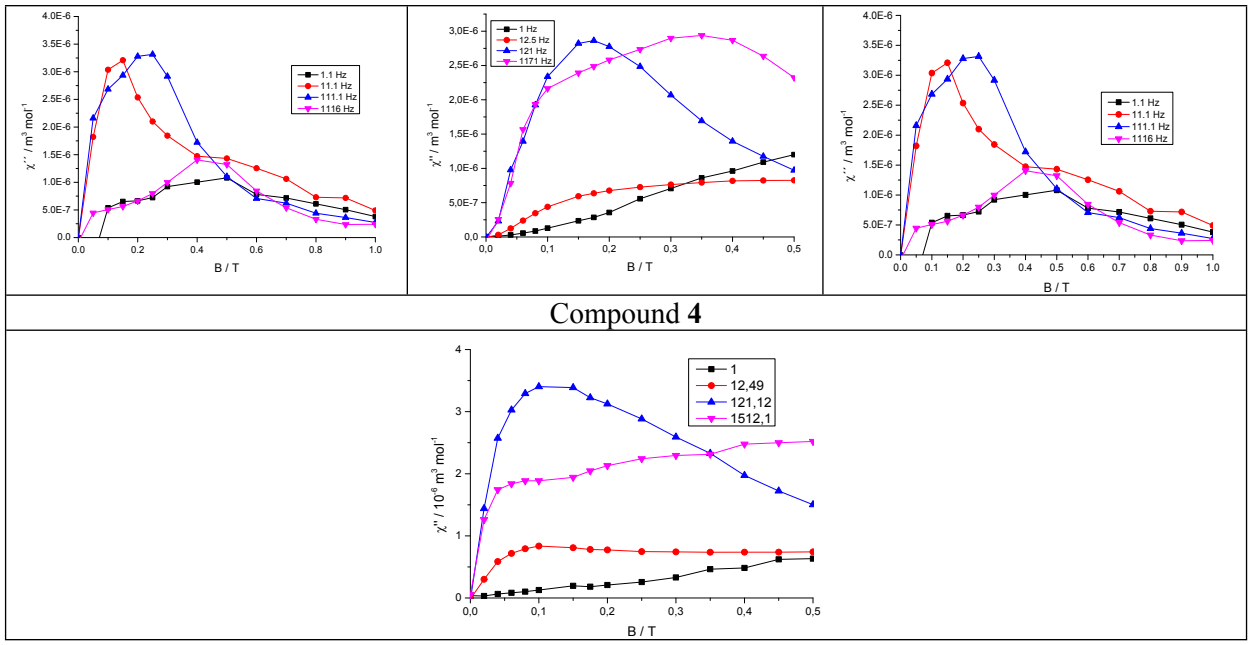

Figure S4.1 DC field dependence for a set of fixed frequencies at 2 K. Solid lines are only guides for the eyes.

Parameters of AC susceptibility magnetic measurements of **1-4** are listed inTable S4.1. In-phase (χ') and out-of-phase (χ'') components of AC susceptibility have been recorded at the given temperatures upon the oscillating magnetic field of different frequency.

Table S4.1 Conditions of AC magnetic experiments for compounds **1-4.**

	B_{DC} / T	B_{AC} / mT	Temperature range	Frequency range
1	0.150	3.8	1.8-4.9 K (33 steps)	1 Hz -1488.1 Hz (20 steps)
2	0.150	3.5	2.0-3.6 K (9 steps)	1 Hz -1512 Hz (32 steps)
3	0.050	3.8	1.9-2.7 K (9 steps)	1 Hz -1488.1 Hz (20 steps)
3	0.125	3.8	1.9-2.8 K (10 steps)	1 Hz -1488.1 Hz (20 steps)
3	0.200	3.8	1.9-2.7 K (9 steps)	1 Hz -1488.1 Hz (20 steps)
3	0.300	3.8	1.9-2.5 K (7 steps)	1 Hz -1488.1 Hz (20 steps)
4	0.100	3.5	2.0-5.2 (17 steps)	1 Hz -1512 Hz (32 steps)

Collected sets of χ' and χ'' susceptibilities (20 χ' and 20 χ'' for **1** and **3** or 32 χ' and 32 χ'' for **2**;) at each temperature were fitted using the formulas for one-set (**1**, **2**; eq. S1 and S2) or two-set (**3**; eq. S3 and S4) Debye model.

$$\chi'(\omega) = \chi_S + (\chi_T - \chi_S)\frac{1+(\omega\tau)^{(1-\alpha)}\sin(\pi\alpha/2)}{1+2(\omega\tau)^{(1-\alpha)}\sin(\pi\alpha/2)+(\omega\tau)^{(2-2\alpha)}} \quad \textbf{(S1)}$$

$$\chi''(\omega) = (\chi_T - \chi_S)\frac{(\omega\tau)^{(1-\alpha)}\cos(\pi\alpha/2)}{1+2(\omega\tau)^{(1-\alpha)}\sin(\pi\alpha/2)+(\omega\tau)^{(2-2\alpha)}} \quad \textbf{(S2)}$$

$$\chi'(\omega) = \chi_S + (\chi_{T1} - \chi_S)\frac{1 + (\omega\tau_1)^{(1-\alpha_1)}\sin(\pi\alpha_1/2)}{1 + 2(\omega\tau_1)^{(1-\alpha_1)}\sin(\pi\alpha_1/2) + (\omega\tau_1)^{(2-2\alpha_1)}} + (\chi_{T2} - \chi_{T1})\frac{1 + (\omega\tau_2)^{(1-\alpha_2)}\sin(\pi\alpha_2/2)}{1 + 2(\omega\tau_2)^{(1-\alpha_2)}\sin(\pi\alpha_2/2) + (\omega\tau_2)^{(2-2\alpha_2)}} \quad \textbf{(S3)}$$

$$\chi''(\omega) = (\chi_{T1} - \chi_S)\frac{(\omega\tau_1)^{(1-\alpha_1)}\cos(\pi\alpha_1/2)}{1 + 2(\omega\tau_1)^{(1-\alpha_1)}\sin(\pi\alpha_1/2) + (\omega\tau_1)^{(2-2\alpha_1)}} + (\chi_{T2} - \chi_{T1})\frac{(\omega\tau_2)^{(1-\alpha_2)}\cos(\pi\alpha_2/2)}{1 + 2(\omega\tau_2)^{(1-\alpha_2)}\sin(\pi\alpha_2/2) + (\omega\tau_2)^{(2-2\alpha_2)}} \quad \textbf{(S4)}$$

Four (for one relaxation channel) or seven (for two relaxation channels) free parameters can be retrieved reliably by using 40 (**1**, **3**) or 64 (**2, 4**) experimental data points for each temperature

Table S4.2 Parameters of the extended Debye model for **1** (two relaxation processes) at B_{DC} = 0.15 T.

T **/K**	$\chi_S/10^{-6}$ **m^3 mol^{-1}**	$\chi_T/10^{-6}$ **m^3 mol^{-1}**	$\alpha/10^{-2}$	$\tau/10^{-4}$**s**	***T*** **/K**	$\chi_S/10^{-6}$ **m^3 mol^{-1}**	$\chi_T/10^{-6}$ **m^3 mol^{-1}**	$\alpha/10^{-2}$	$\tau/10^{-4}$**s**
1.8	0.70	13.79	23.87	20.87	3.4	0.88	7.94	12.68	4.35
1.9	0.66	13.15	23.75	19.03	3.5	0.90	7.73	12.04	3.85
2.0	0.64	12.64	23.77	17.02	3.6	0.98	7.53	10.13	3.53
2.1	0.63	12.11	23.32	15.46	3.7	0.82	7.34	9.63	3.02
2.2	0.61	11.79	23.66	14.45	3.8	0.86	7.17	8.91	2.68
2.3	0.55	11.30	24.05	12.93	3.9	0.93	7.00	7.27	2.44
2.4	0.59	10.86	22.63	11.70	4.0	0.94	6.84	6.24	2.17
2.5	0.58	10.50	22.86	10.69	4.1	1.01	6.68	4.41	1.96
2.6	0.63	10.11	21.60	9.76	4.2	1.00	6.53	4.49	1.73
2.7	0.61	9.79	21.73	8.84	4.3	0.99	6.40	4.21	1.53
2.8	0.72	9.46	19.64	8.06	4.4	0.88	6.26	4.12	1.33
2.9	0.65	9.20	19.80	7.27	4.5	0.88	6.15	3.69	1.17
3.0	0.78	8.91	16.95	6.66	4.6	0.88	6.01	3.44	1.03
3.1	0.76	8.63	16.75	5.99	4.7	0.79	5.90	3.58	0.89
3.2	0.81	8.39	14.99	5.32	4.8	0.76	5.78	3.37	0.79
3.3	0.87	8.15	13.37	4.84	4.9	0.90	5.67	2.07	0.72

Compound **1** @ 0.15 T

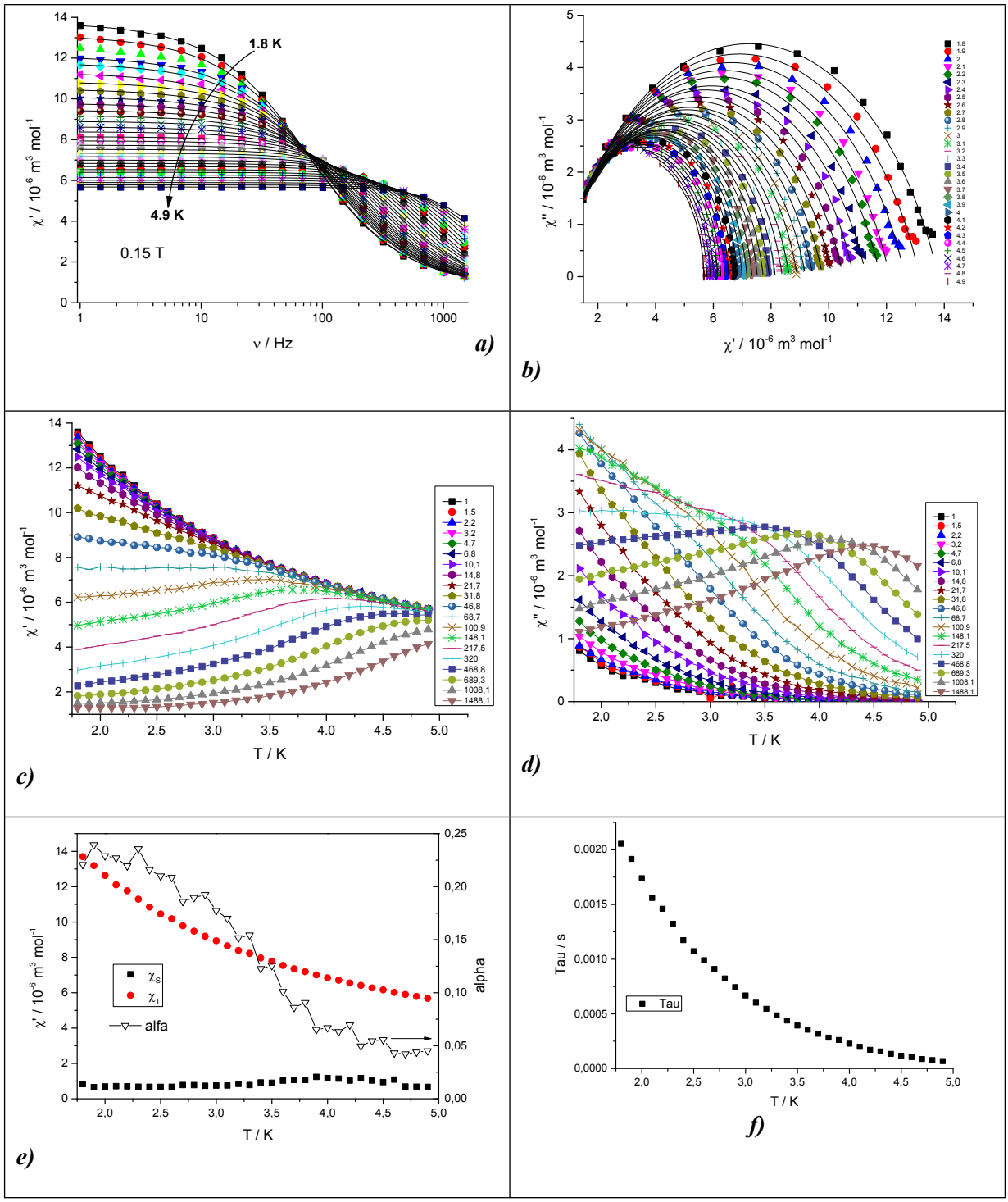

Figure S4.2 AC susceptibility data for **1** recorded at B_{DC}=0.15 T: Frequency dependent in-phase χ' component of AC susceptibility (***a***), Cole-cole diagram (***b***), temperature dependence of in-phase χ'(***c***) and out-of-phase χ'' (***d***) components of AC susceptibility (solid lines are only guides for the eyes), temperature evolution of χ_T, χ_S, α (***e***) and τ (***f***) parameters obtained from two-component Debye model (eq. S1 and S2).

Table S4.3 Result of the fitting procedure for AC susceptibility components of **2** at B_{DC}=0.15 T.

T **/K**	χ_S**/10^{-6} m^3 mol^{-1}**	χ_T**/10^{-6} m^3 mol^{-1}**	α**/10^{-2}**	τ**/10^{-4} s**
2.0	1.93	11.23	15.33	4.80
2.2	1.68	10.58	16.53	3.63

2.4	1.56	9.75	15.84	2.53
2.6	1.48	9.13	14.40	1.81
2.8	1.53	8.54	11.67	1.30
3.0	1.60	8.05	9.43	0.95
3.2	1.83	7.60	6.75	0.73
3.4	1.91	7.20	4.33	0.55
3.6	1.22	6.85	4.98	0.34

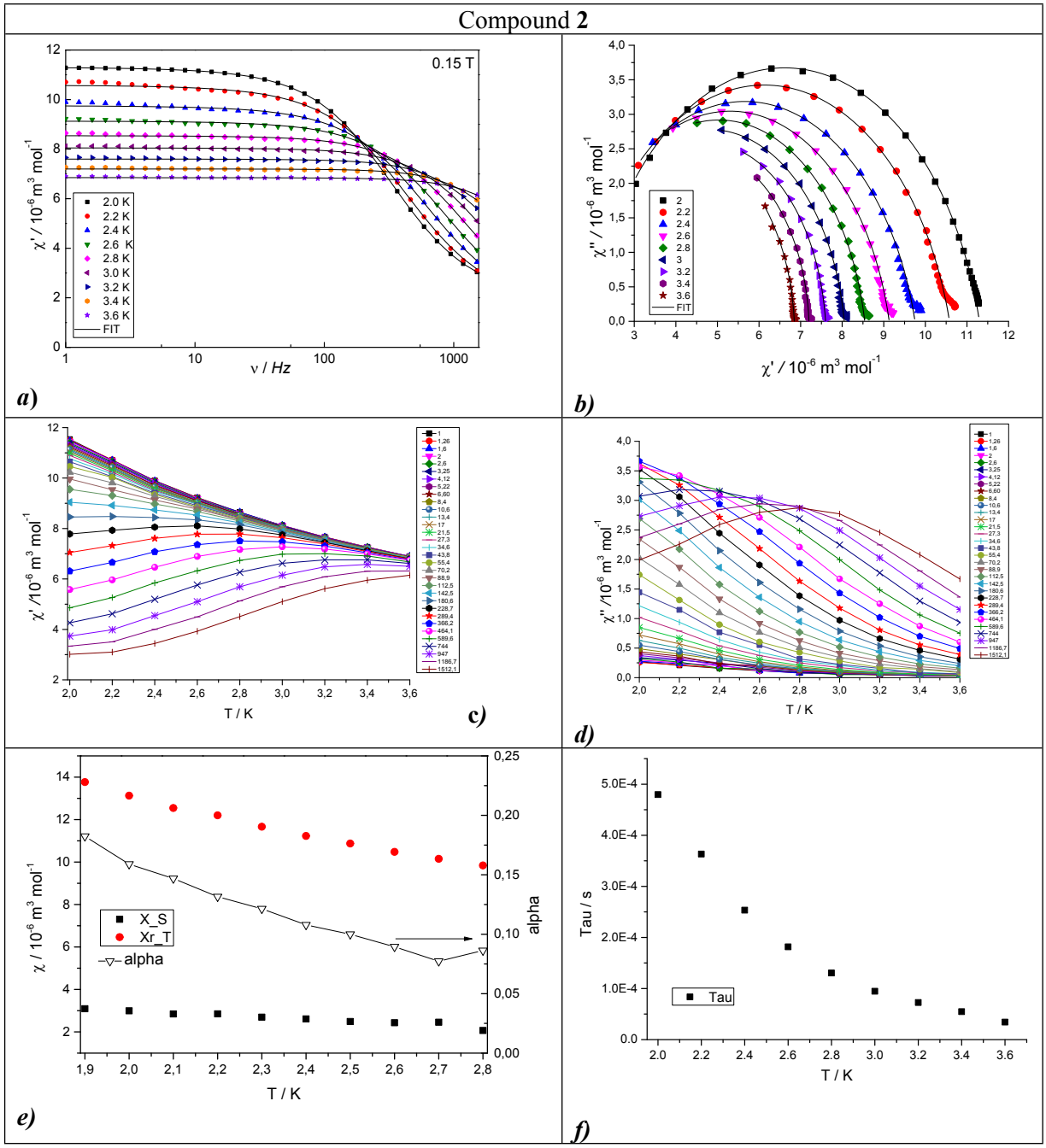

Figure S4.3 AC susceptibility data for **2** recorded at B_{DC}=0.15 T: Frequency dependent in-phase χ' component of AC susceptibility (***a***), Cole-cole diagram (***b***), temperature dependence of in-phase χ'(***c***) and out-of-phase χ'' (***d***) components of AC susceptibility (solid lines are only guides for the eyes), temperature evolution of χ_T, χ_S, α (***e***) and τ (***f***) parameters obtained from two-component Debye model (eq. S1 and S2).

Table S4.4 Result of the fitting procedure for AC susceptibility components of **3.**

B/T	T /K	$\chi_S/10^{-6}$ m^3 mol^{-1}	$\chi_{T1}/10^{-6}$ m^3 mol^{-1}	$\chi_{T2}/10^{-6}$ m^3 mol^{-1}	$\alpha_1/10^{-2}$	$\alpha_2/10^{-2}$	$\tau_{01}/10^{-2}$s	$\tau_{02}/10^{-4}$ s
0.05	1.9	8.69	-	14.32	-	7.49	-	5.14
	2.0	8.24	-	13.64	-	6.81	-	4.17
	2.1	7.81	-	13.05	-	7.20	-	3.33
	2.2	7.64	-	12.65	-	5.00	-	2.88
	2.3	7.28	-	12.07	-	4.39	-	2.23
	2.4	6.94	-	11.62	-	4.60	-	1.74
	2.5	6.76	-	11.18	-	3.57	-	1.40
	2.6	6.52	-	10.79	-	3.77	-	1.10
	2.7	6.33	-	10.41		2.94	-	0.88
0.125	1.9	3.09	-	13.77	-	18.23	-	6.00
	2.0	2.99	-	13.13	-	15.90	-	4.81
	2.1	2.84	-	12.55	-	14.69	-	3.82
	2.2	2.85	-	12.20	-	13.15	-	3.30
	2.3	2.69	-	11.66	-	12.14	-	2.53
	2.4	2.61	-	11.23	-	10.79	-	2.00
	2.5	2.49	-	10.87	-	10.00	-	1.58
	2.6	2.43	-	10.48	-	8.94	-	1.25
	2.7	2.46	-	10.15	-	7.73	-	1.01
	2.8	2.06	-	9.84	-	8.63	-	0.75
0.2	1.9	1.22	3.89	13.94	24.61	19.37	2.75	3.97
	2.0	1.75	3.89	13.18	21.05	15.00	2.27	3.72
	2.1	1.83	3.72	12.66	22.42	12.55	2.12	3.18
	2.2	1.88	3.59	12.30	23.61	10.74	1.94	2.83
	2.3	1.88	3.36	11.80	25.84	9.64	1.99	2.30
	2.4	1.85	3.09	11.33	25.43	8.65	2.09	1.88
	2.5	1.55	2.60	10.96	27.99	10.01	2.59	1.45
	2.6	1.63	2.56	10.58	30.08	8.32	2.30	1.19
	2.7	1.77	2.55	10.26	30.36	8.72	2.74	0.97
0.3	1.9	0.81	5.46	13.13	22.80	20.12	2.92	2.36
	2.0	0.89	4.93	12.56	23.24	18.21	2.49	2.17
	2.1	0.67	4.02	12.08	22.06	19.13	2.50	1.88
	2.2	0.70	3.72	11.77	23.11	18.10	2.32	1.73
	2.3	0.75	3.38	11.30	23.60	16.41	2.37	1.46
	2.4	0.81	3.16	10.94	25.93	14.64	2.37	1.24
	2.5	0.85	2.96	10.61	27.56	12.88	2.42	1.06

Compound **3** @ 0.05 T

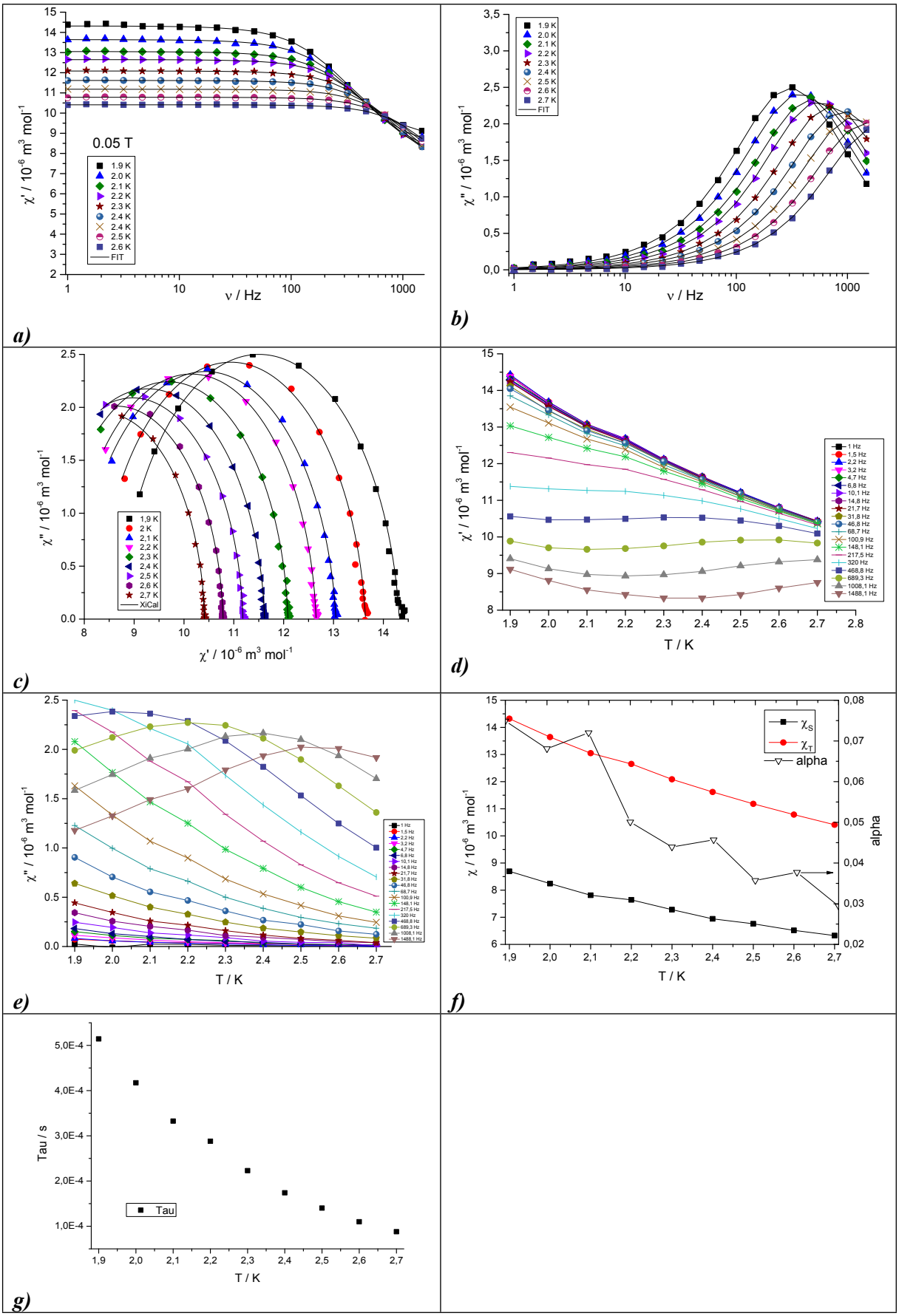

Figure S4.4 AC susceptibility data for **3** recorded at B_{DC}=0.05 T: Frequency dependence of in-phase χ' (***a***) and out-of-phase χ'' (***b***) AC susceptibility components (solid lines present fits using the two-

component Debye's model, eq. S3 and S4), Cole-Cole diagram (*c*), temperature dependence of in-phase χ' (***d***) and out-of-phase χ'' (***e***) AC susceptibility components (solid lines are only guides for the eyes) and temperature evolution of χ_{T1}, χ_{T2}, χ_S, α_1, α_2 (***f***) and τ_1, τ_2 (***g***) parameters obtained from two-component Debye model (eq. S1 and S2).

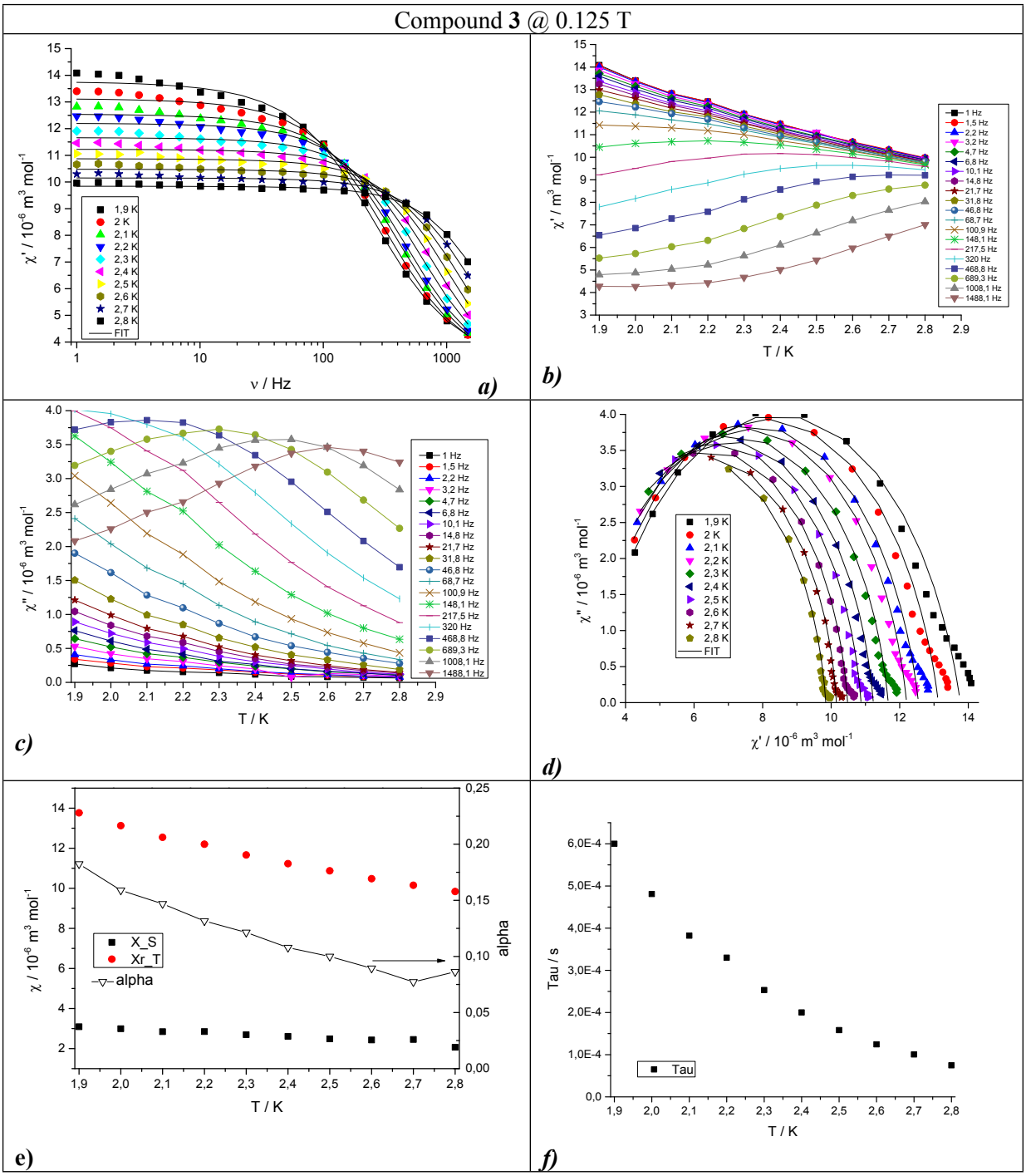

Figure S4.5 AC susceptibility data for **3** recorded at B_{DC}=0.125 T: Frequency dependent in-phase χ' component of AC susceptibility (***a***), temperature dependence of in-phase χ'(***b***) and out-of-phase χ'' (***c***) components of AC susceptibility (solid lines are only guides for the eyes), Cole-Cole diagram (*d*), temperature evolution of χ_T, χ_S, α, (***e***) and τ (***f***) parameters obtained from two-component Debye model (eq. S1 and S2).

Compound **3** @ 0.2 T

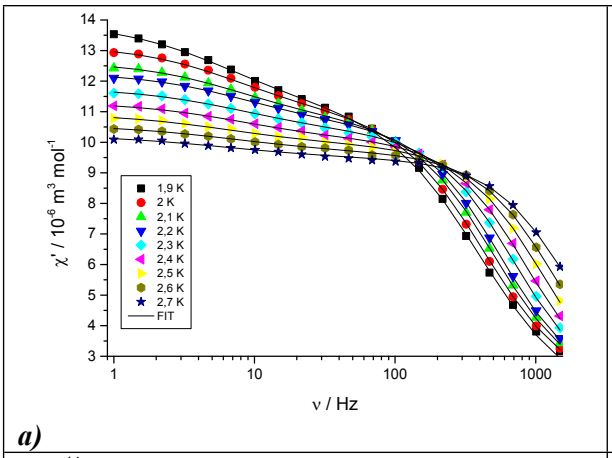
χ' / 10-6 m3 mol-1
ν / Hz
1,9 K
2 K
2,1 K
2,2 K
2,3 K
2,4 K
2,5 K
2,6 K
2,7 K
FIT

a)

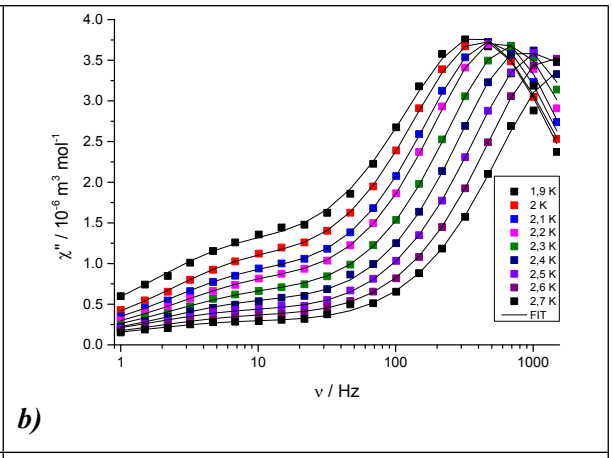
χ'' / 10-6 m3 mol-1
ν / Hz
1,9 K
2 K
2,1 K
2,2 K
2,3 K
2,4 K
2,5 K
2,6 K
2,7 K
FIT

b)

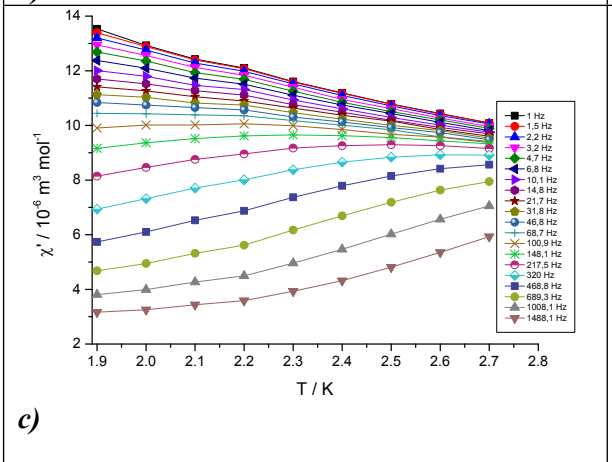
χ' / 10-6 m3 mol-1
T / K
1 Hz
1,5 Hz
2,2 Hz
3,2 Hz
4,7 Hz
6,8 Hz
10,1 Hz
14,8 Hz
21,7 Hz
31,8 Hz
46,8 Hz
68,7 Hz
100,9 Hz
148,1 Hz
217,5 Hz
320 Hz
468,8 Hz
689,3 Hz
1008,1 Hz
1488,1 Hz

c)

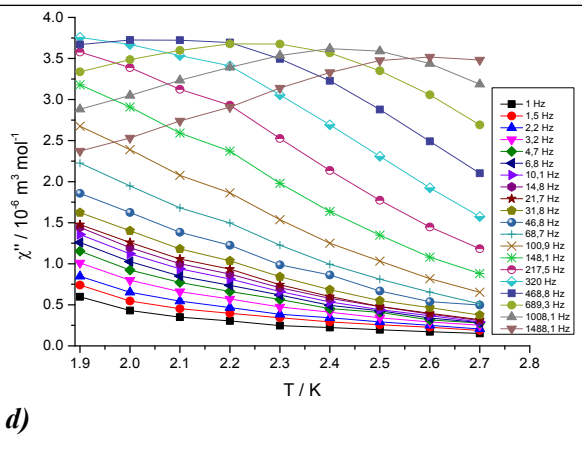
χ'' / 10-6 m3 mol-1
T / K
1 Hz
1,5 Hz
2,2 Hz
3,2 Hz
4,7 Hz
6,8 Hz
10,1 Hz
14,8 Hz
21,7 Hz
31,8 Hz
46,8 Hz
68,7 Hz
100,9 Hz
148,1 Hz
217,5 Hz
320 Hz
468,8 Hz
689,3 Hz
1008,1 Hz
1488,1 Hz

d)

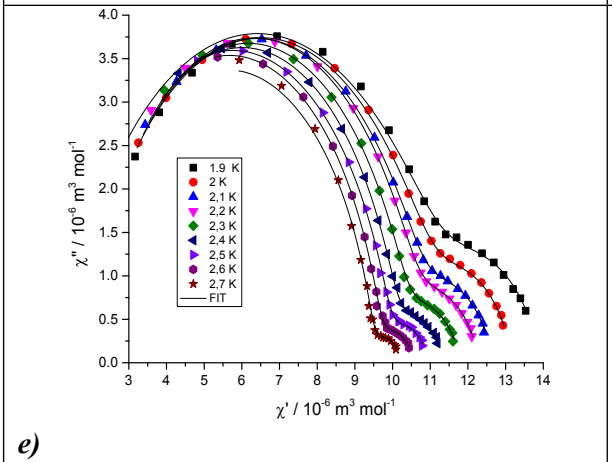
χ'' / 10-6 m3 mol-1
χ' / 10-6 m3 mol-1
1.9 K
2 K
2,1 K
2,2 K
2,3 K
2,4 K
2,5 K
2,6 K
2,7 K
FIT

e)

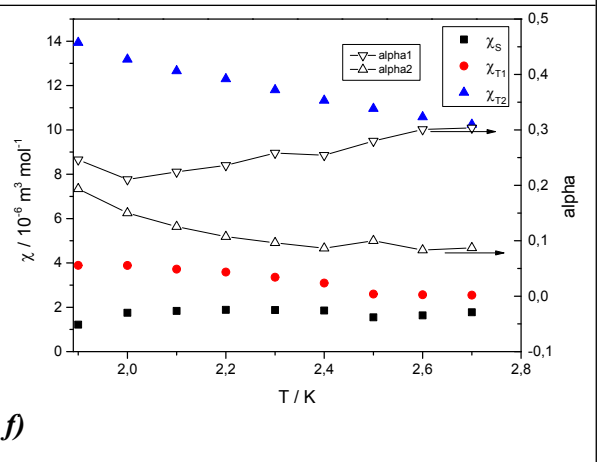
χ / 10-6 m3 mol-1
T / K
alpha
alpha1
alpha2
χS
χT1
χT2

f)

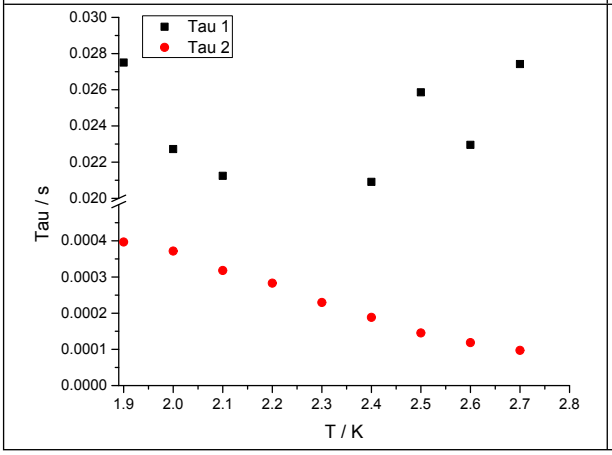
Tau / s
T / K
Tau 1
Tau 2

g)	

Figure S4.6 AC susceptibility data for **3** recorded at B_{DC}=0.2 T: Frequency dependence of in-phase χ' (***a***) and out-of-phase χ'' (***b***) AC susceptibility components (solid lines present fits using the two-component Debye's model, eq.S3 and S4). Temperature dependence of in-phase χ' (***c***) and out-of-phase χ'' (***d***) AC susceptibility components (solid lines are only guides for the eyes), Cole-Cole diagram (***e***) and temperature evolution of χ_{T1}, χ_{T2}, χ_S, α_1, α_2 (***f***) and τ_1, τ_2 (***g***) parameters obtained from two-component Debye model (eq. S3 and S4).

Compound **3** @ 0.3 T

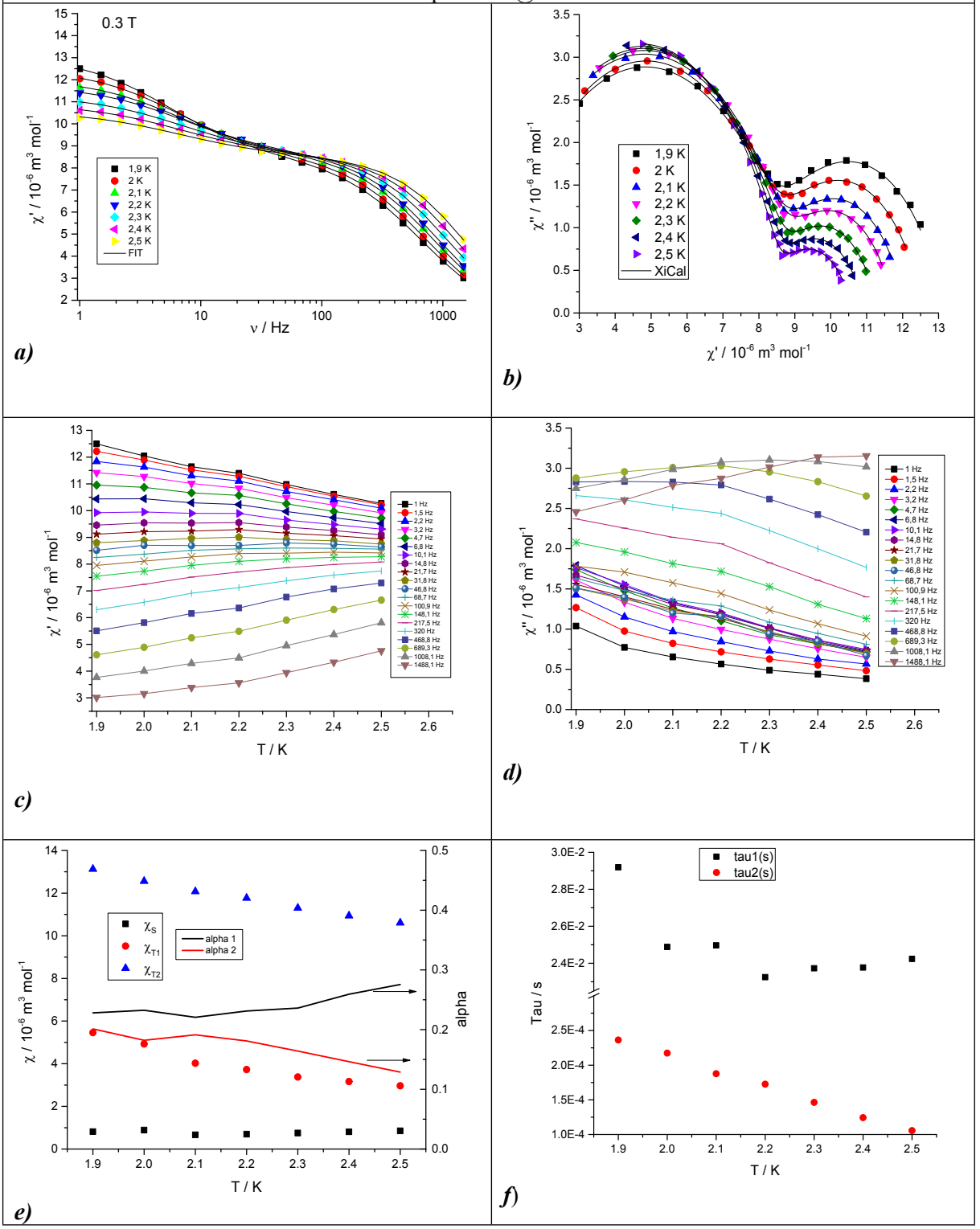

Figure S4.7 AC susceptibility data for **3** recorded at B_{DC}=0.3 T: Frequency dependent in-phase χ' component of AC susceptibility (***a***), Cole-cole diagram (***b***), temperature dependence of in-phase χ'(***c***) and out-of-phase χ'' (***d***) components of AC susceptibility (solid lines are only guides for the eyes), temperature evolution of χ_{T1}, χ_{T2}, χ_S, α_1, α_2 (***e***) and τ_1, τ_2 (***f***) parameters obtained from two-component Debye model (eq. S3 and S4).

Table S4.5 Result of the fitting procedure for AC susceptibility components of **4** at B_{DC}=0.15 T.

T **/K**	$\chi_S/10^{-6}$ **m^3 mol^{-1}**	$\chi_T/10^{-6}$ **m^3 mol^{-1}**	$\alpha/10^{-2}$	$\tau/10^{-4}$ **s**
2.0	1.14	11.57	19.04	6.53
2.2	1.04	10.74	19.18	5.06
2.4	1.04	9.81	18.77	3.77
2.6	0.89	9.11	18.77	2.83
2.8	0.88	8.49	18.16	2.17
3.0	0.99	7.98	17.40	1.77
3.2	1.18	7.54	15.44	1.50
3.4	0.92	7.13	16.76	1.12
3.6	0.88	6.76	16.28	0.92
3.8	1.39	6.43	13.23	0.87
4.0	1.61	6.14	10.75	0.82
4.2	1.69	5.87	9.48	0.70
4.4	1.66	5.62	7.78	0.59
4.6	1.82	5.40	6.46	0.54
4.8	1.87	5.19	6.69	0.48
5.0	1.68	5.00	4.11	0.40
5.2	1.60	4.83	3.75	0.33

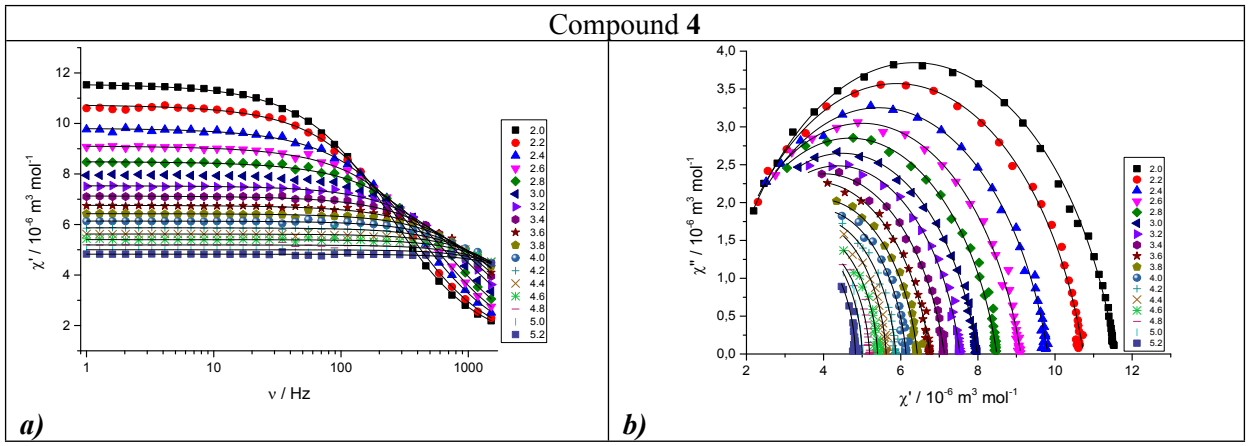

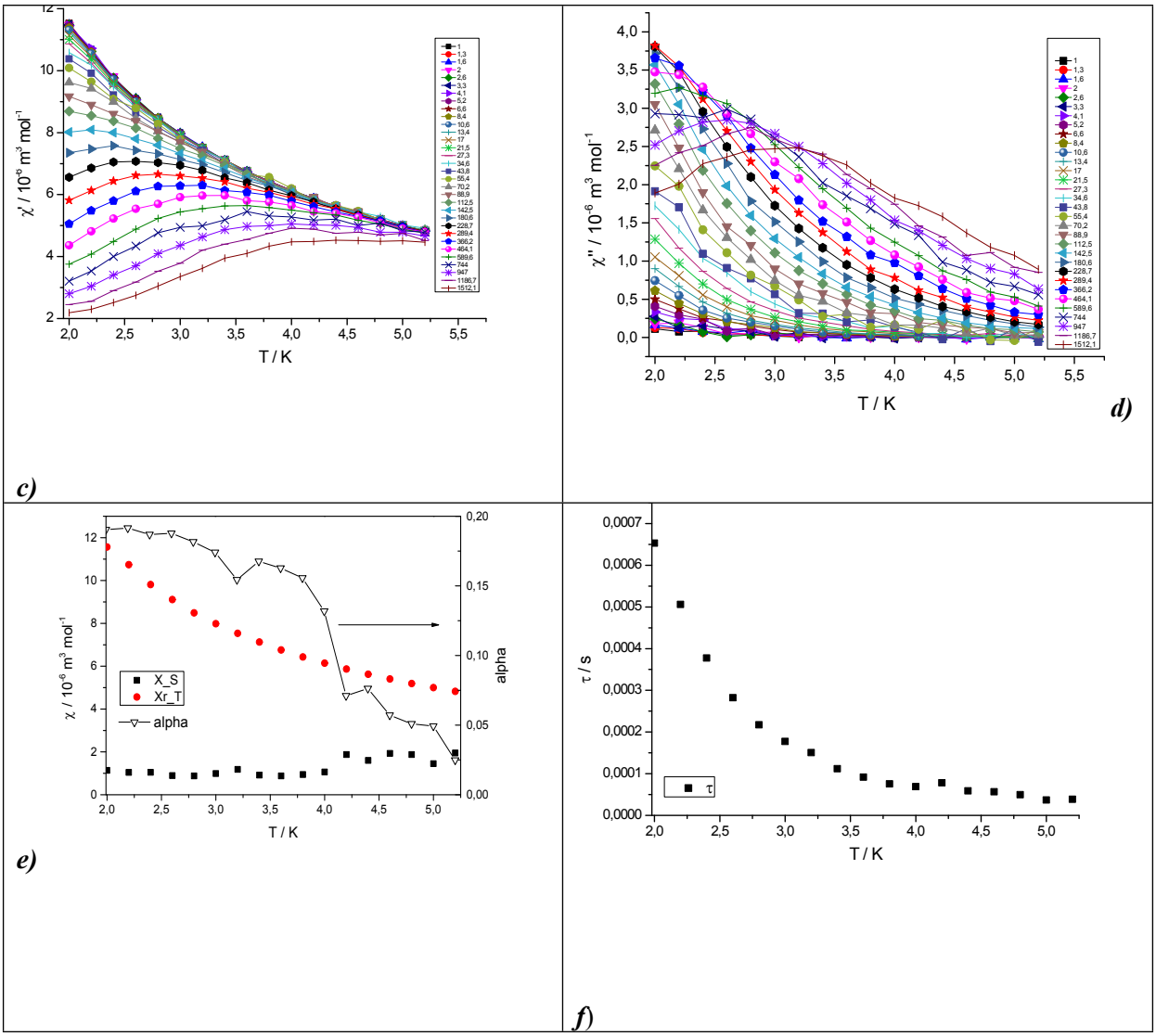

Figure S4.8 AC susceptibility data for **4** recorded at B_{DC}=0.1 T: Frequency dependent in-phase χ' component of AC susceptibility (***a***), Cole-cole diagram (***b***), temperature dependence of in-phase χ'(***c***) and out-of-phase χ'' (***d***) components of AC susceptibility (solid lines are only guides for the eyes), temperature evolution of χ_T, χ_S, α (***e***) and τ (***f***) parameters obtained from two-component Debye model (equations S1 and S2).

Table S4.6 Relaxation parameters for compounds **1** and **2** using the single Orbach, single Raman model and their combinations.

	Model	**B_{DC} / T**	***U*/k_B / K**	**τ_0/s**	***C* / K^{-n} s^{-1}; n**	***AB^m* / *T*$^{-m}$ K^{-1} s^{-1}**	**R^2**
1	Orbach[a]	0.15	25.75±0.71	(3.71±0.61)10^{-7}	-	-	0.9924
1	Raman[a]	0.15	-	-	1.20±0.20; 5.91±0.11	-	0.9966
1	Orbach+Direct	0.15	24.61±0.88	(5.87±1.22)10^{-7}	-	307.75±9.39	0.9941
1	Raman+Direct	0.15	-	-	0.79±0.14; 6.07±0.12	271.81±6.73	0.9982
2	Orbach[b]	0.15	12.79±0.77	(1.23±0.34)10^{-6}	-		0.9753
2	Raman[b]	0.15	-	-	68.76±12.01; 4.61±0.16	-	0.9913
2	Orbach+Direct	0.15	18.92±1.35	(2.28±0.92)10^{-7}	-	893.83±93.51	0.9945
2	Raman+Direct	-	-	-	14.93±7.06; 5.78±0.38	632.85±121.05	0.9964

[a] for the temperature range 3.9 K -4.9 K; [b] for the temperature range 2.2 K -3.6 K;

Table S4.7 Relaxation parameters for compound **3** using the single Orbach, single Raman model and their combinations.

	Model	**B_{DC} / T**	**U_{eff}/k_B / K**	**τ_0/s**	**C / K^{-n} s^{-1}; n**	**AB^m / T^{-m} K^{-1} s^{-1}**	**R^2**
3	Orbach[a]	0.05	14.03±0.29	$(4.98\pm0.60)10^{-7}$	-	-	0.9978
3	Raman[a]	0.05	-	-	36.58±1.65; 5.77±0.05	-	0.9996
3	Orbach+Direct	0.05	19.10±0.92	$(9.22\pm3.16)10^{-8}$	-	797.38±49.03	0.9984
3	Raman+Direct	0.05	-	-	7.67±2.77; 7.19±0.36	626.32±67.30	0.9987
3	Orbach[a]	0.125	14.87±0.53	$(3.97\pm0.86)10^{-7}$	-	-	0.9924
3	Raman[a]	0.125			26.02±3.25; 6.01±0.14	-	0.9969
3	Orbach+Direct	0.125	20.06±0.93	$(7.13\pm2.47)10^{-8}$	-	713.01±45.49	0.9980
3	Raman+Direct	0.125	-	-	5.37±1.76; 7.44±0.31	558.97±54.79	0.9986
3	Orbach[c]	0.2	12.83±0.43	$(8.57\pm1.54)10^{-7}$	-	-	0.9943
3	Raman[c]	0.2	-	-	53.90±5.78; 5.28±0.12	-	0.9975
3	Orbach+Direct	0.2	23.46±1.44	$(2.31\pm1.24)10^{-8}$	-	1196.11±65.56	0.9974
3	Raman+Direct	0.2	-	-	1.04±0.71; 8.96±0.68	1115.23±65.56	0.9963
3	Orbach[d]	0.3	7.11±0.53	$(6.43\pm1.55)10^{-6}$	-	-	0.9727
3	Raman[d]	0.3	-	-	488.28±76.09; 3.20±0.19	-	0.9824
3	Orbach+Direct	0.3	21.22±2.39	$(4.77\pm4.44)10^{-6}$	-	2067.28±72.40	0.9967
3	Raman+Direct	0.3	-	-	2.02±1.96; 8.43±1.01	1982(99)	0.9966

[a]for the temperature range 2.2 K-2.7 K; [b]for the temperature range 2.2 K-2.8 K; [c]for the temperature range 2.2 K-2.8 K; [d]for the temperature range 2.0 K-2.5 K;

Table S4.8 Relaxation parameters for compounds **4** using the single Orbach, single Raman model and their combinations.

	Model	**B_{DC} / T**	**U_{eff}/k_B / K**	**τ_0/s**	**C / K^{-n} s^{-1}; n**	**R^2**
4	Orbach	0.1	9.54±0.29	$(6.70\pm0.61)10^{-6}$	-	0.9856
4	Raman	0.1	-	-	201.44±21.96; 3.00±0.09	0.9872

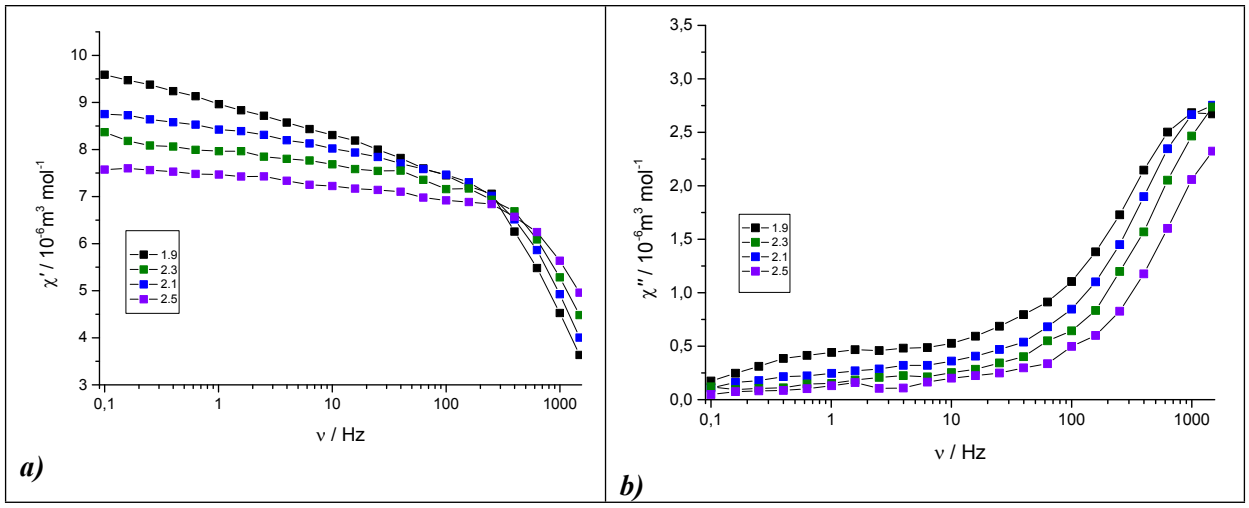

Figure S4.9 AC susceptibility data for compound **3** diluted in eicosane and recorded at B_{DC}=0.3 T.

S5 Magneto-Structural Correlations

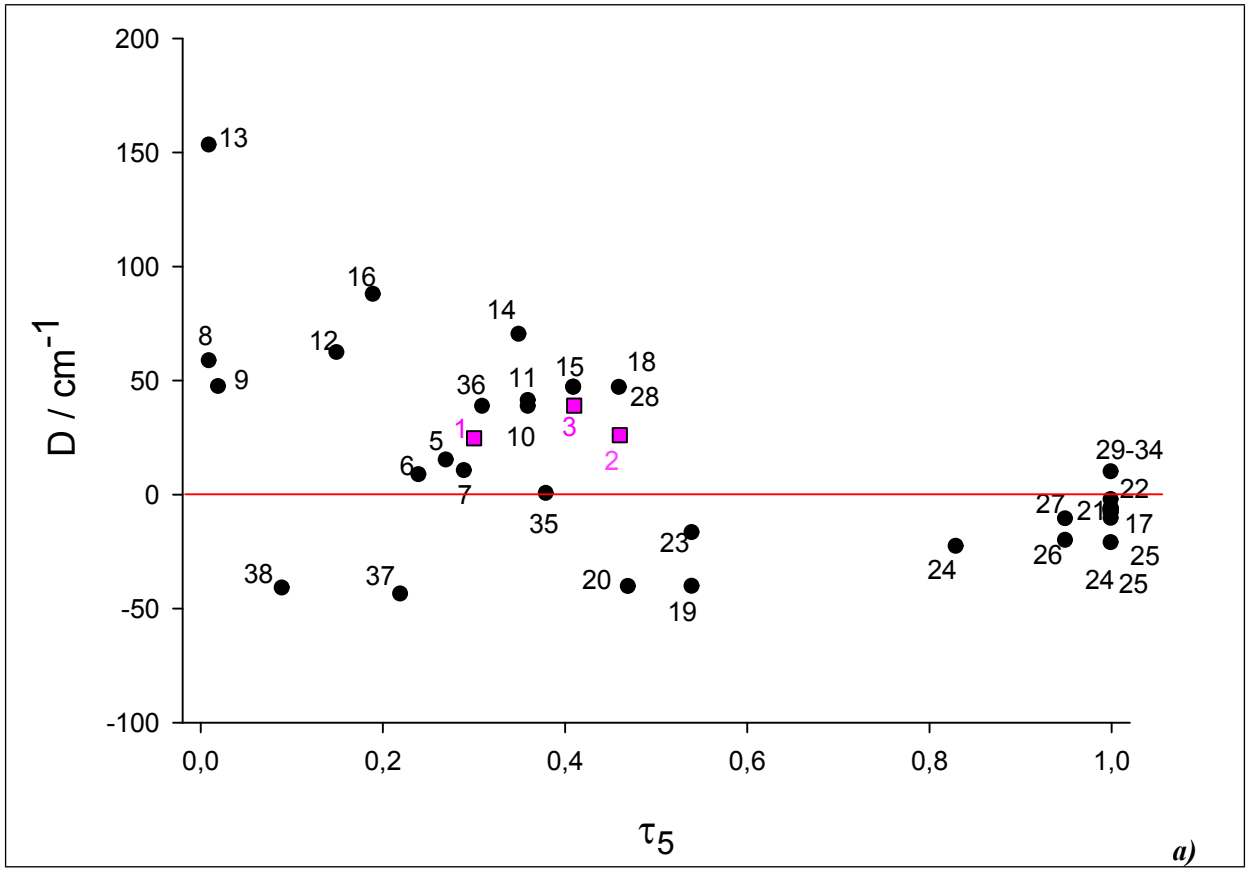

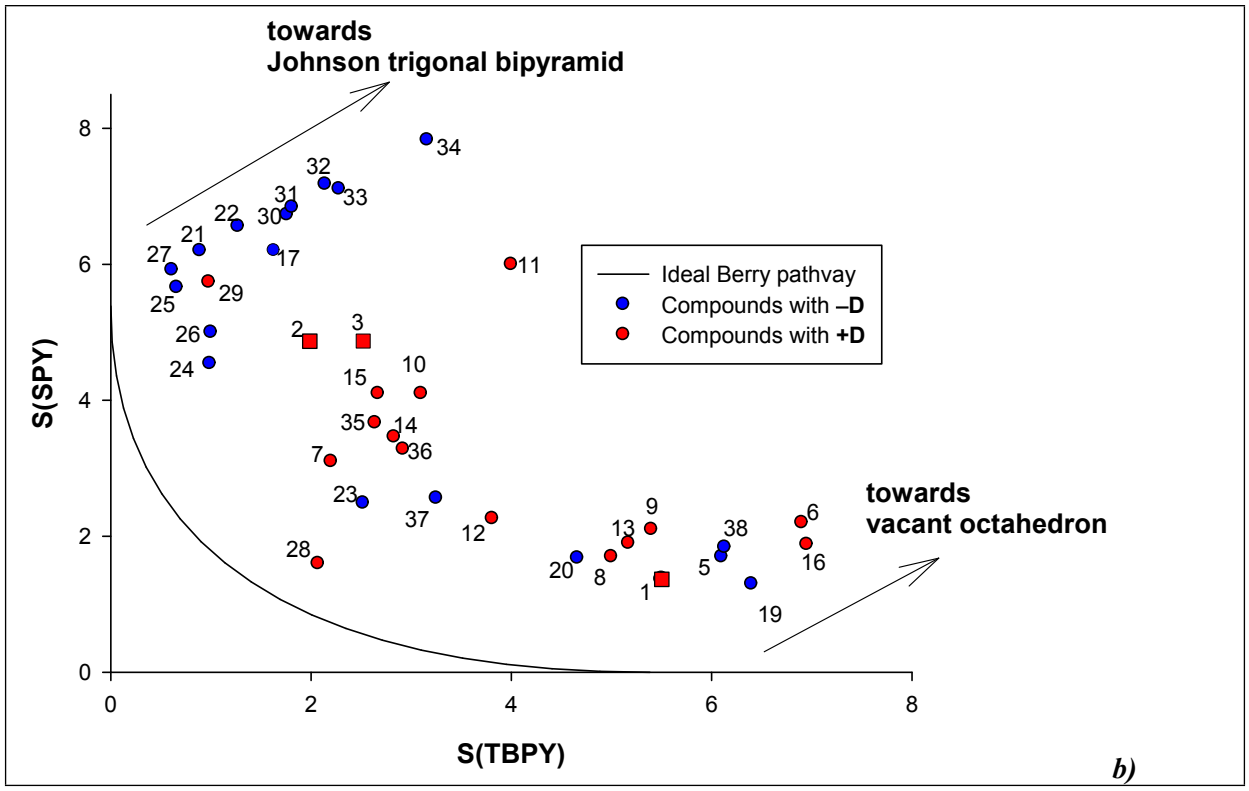

Figure S5.1 Magneto-structural correlations for 37 pentacoordinated Co(II) SIMs. a) correlation between Addison τ_5 parameter and axial zero-field splitting D parameter; b) Shape map for trigonal bipyramid (TBPY) and square pyramid (SPY). The red and blue color indicate the positive and negative values of D, respectively, found in the corresponding compounds. **1-3** – this work; **5-7**,[9] **8-9**,[10] **10-11**,[11] **12-16**,[12,13] **17,**[14] **18**,[15] **19-20**,[16] **21-22**,[17] **23**,[18] **24**,[19] **25-27**,[20] **8**,[21] **29-34**,[22] **35-38**,[23]

References

1. L. Palatinus and G. Chapuis, J. Appl. Crystallogr., 2007, 40, 786
2. G. M. Sheldrick, Acta Crystallogr., 2015, A71, 3.
3. G. M. Sheldrick, Acta Crystallogr., 2015, C71, 3.
4. J. Koziskova, F. Hahn, J. Richter and J. Kozisek, Acta Chim. Slovaca, 2016, 9, 136.
5. C. F. Macrae, I. J. Bruno, J. A. Chisholm, P. R. Edgington, P. McCabe, E. Pidcock, L. Rodriguez-Monge, R. Taylor, J. van der Streek and P. A. Wood, J. Appl. Crystallogr., 2008, 41, 466.
6. R. Boča, Theoretical Foundations of Molecular Magnetism, Elsevier, Amsterdam, 1999.
7. M. A. Halcrow, *Coord. Chem. Rev.,* 2009, ***253*****,** 2493.
8. (*a*) P. Guionneau, M. Marchivie, G. Bravic, J.-F. Létard and D. Chasseau, *Top. Curr. Chem.*, 2004, ***234***, 97; (*b*) M. A. Halcrow, *Chem. Soc. Rev*., 2011, **40**, 4119.
9. A. K: Mondal, T. Goswami, A. Misra and S. Konar, *Inorg. Chem.*, 2017, **56**, 6870
10. C. Rajnák, F. Varga, J. Titiš, J. Moncoľ and R. Boča, *Eur. J. Inorg. Chem.,* 2017, **13**, 1915
11. A. Switlicka, B. Machura, M. Penkala, A. Bienko, D. C. Bienko, J. Titis, C. Rajnak, R. Boca, A. Ozarowski and M. Ozerov, Inorg. Chem., 2018, 57, 12740
12. C. Rajnák, J. Titiš, J. Miklovic, G. E. Kostakis, O. Fuhr, M. Ruben, R. Boca Polyhedron 2017 126 174-183.
13. C. Rajnák, J. Titiš, O. Fuhr, M. Ruben and R. Boča, Inorg. Chem., 2014, 53, 8200.
14. D. Schweinfurth, M. G. Sommer, M. Atanasov, S. Demeshko, S. Hohloch, F. Meyer, F. Neese and B. Sarkar J. Am. Chem. Soc. 2015, 137, 1993−2005
15. C. Rajnák, J. Titiš, I. Šalitroš, R. Boča, O. Fuhr, M. Ruben Polyhedron 2013, 65, 122–128.

16. T. Jurca, A. Farghal, P.-H. Lin, I. Korobkov, M. Murugesu, D. S. Richeson J. Am. Chem. Soc. 2011, 133, 15814 —15817
17. R. Ruamps, L. J. Batchelor, R. Guillot, G. Zakhia, A.-L. Barra, W. Wernsdorfer, N. Guihéry and T. Mallah, Chem. Sci., 2014,5, 3418-3424
18. I. Nemec, R. Marx, R. Herchel, P. Neugebauer, J. van Slageren, Z. Trávníček, Dalton Trans., 2015, 44, 15014
19. F. Shao, B. Cahier, N. Guihéry, E. Rivière, R. Guillot, A.-L. Barra, Y. Lan, W. Wernsdorfer, V. E. Campbell and T. Mallah, Chem. Commun., 2015,51, 16475-16478
20. F. Shao, B. Cahier, E. Rivière, R. Guillot, N. Guihéry, V. E. Campbell and T. Mallah Inorg. Chem. 2017, 56, 1104-1111
21. B. Cahier, M. Perfetti, G. Zakhia, D. Naoufal, F. El-Khatib, R. Guillot, E Riviere, Roberta Sessoli, A.-L. Barra, N. Guihery and T. Mallah, Chem. Eur. J. 2017, 23, 3648 – 3657.
22. T. J. Woods, M. F. Ballesteros-Rivas, S. Gómez-Coca, E. Ruiz and K. R. Dunbar J. Am. Chem. Soc. 2016, 138, 16407−16416
23. I. Nemec, H.Liu, R. Herchel, X. Zhang, and Z. Travnicek Synthetic Metals 215 (2016) 158–163.